57 $(CH_3NH_3)_5Bi_2Cl_{11}$ family

57A Pure compounds

No. 57A-1 $(CH_3NH_3)_5Bi_2Cl_{11}$, Pentakis(methylammonium) undecachlorodibismuthate

(M = 968.27)

1a Ferroelectricity in $(CH_3NH_3)_5Bi_2Cl_{11}$ was discovered by Jakubas et al. in 1989. 89Jak

b

phase	II	I	89Jak
state	F	P	
crystal system	orthorhombic	orthorhombic	
space group	$Pca2_1-C_{2v}^{5}$ [a])	$Pcab-D_{2h}^{15}$ [a])	[a]) 91Lef1
Θ [K]	307.4 [b])		[b]) 94Iwa

For $(CH_3ND_3)_5Bi_2Cl_{11}$, Θ_{II-I} = 308.5 K [c]); see also [d]). [c]) 94Dec, [d]) 95Ish

Existence of monoclinic phase with space group $P112_1-C_2^2$ below 250(10) K was reported by X-ray study.[e]) Corresponding anomaly has been observed only in specific heat. [f]) [g]) [h]) The specific heat anomaly, however, disappeared after the specimen was dried in vacuo at about 100 °C for two days. [f]) [e]) 95Car, [f]) 94Iwa, [g]) 94Str, [h]) 95Str

Phase transition to cation-diffusing phase was observed at 520 K by ^{1}H NMR and DSC. 95Nag

$P_s \parallel [001]$ 89Jak

Transparent. 90Iwa

$\rho = 2.31 \cdot 10^3$ kg m^{-3} at RT. 89Jak

T_{melt} = 590 K. 95Nag

Phase diagram in regard to p: Fig. 57A-1-001; see also 92Mro

$d\Theta_{II-I}/dp = 0.063$ K MPa^{-1}. 95Ges

2a Crystal growth:

1: $(CH_3NH_3)_5Bi_2Cl_{11}$ was synthesized by a reaction of $Bi(OH)_3$ or $(BiO)_2CO_3$ with CH_3NH_3Cl in a large excess of HCl, then purified by repeated recrystallization. Single crystals were grown by slow evaporation of dilute HCl solution at RT. 89Jak, 91Lef2

2: $(CH_3NH_3)_5Bi_2Cl_{11}$ was synthesized in aqueous solution of CH_3NH_3Cl and $BiCl_3$ with a great excess of HCl. Single crystals were grown by slowly cooling the aqueous solution from about 100 °C to 30 °C. 90Iwa

3a Unit cell parameters:

a = 12.924(2) Å, b = 14.034(2) Å, c = 15.364(2) Å at T = 294 K. 91Lef1

a = 13.003(2) Å, b = 14.038(3) Å, c = 15.450(2) Å at T = 349 K. 91Lef1

b Z = 4 in phase I and phase II. 91Lef1

In the following, unusual symmetry operations are adopted for phase II.

They are: x, y, z; $-x, 1/2-y, 1/2+z$; $1/2-x, y, 1/2+z$; $1/2+x, 1/2-y, z$. 91Lef1

Positional and temperature parameters: Table 57A-1-001.

Interatomic distances and angles: Table 57A-1-002, Table 57A-1-003.

Characterization of disorder of methylammonium cations: Table 57A-1-004.

Crystal structure: Fig. 57A-1-002, Fig. 57A-1-003, Fig. 57A-1-004.

Crystal structure analysis at T = 130 K with space group $P112_1-C_2^2$: see 95Car

4 Interaxial angle γ below 270 K: see 95Car

	Thermal expansion: Fig. 57A-1-005; see also	91Pyk, 95Car
5a	Dielectric constant: Fig. 57A-1-006, Fig. 57A-1-007, Fig. 57A-1-008; see also	89Jak
	Curie-Weiss constant: see	89Jak, 90Iwa
	Dielectric dispersion: Fig. 57A-1-009, Fig. 57A-1-010, Fig. 57A-1-011, Fig. 57A-1-012, Fig. 57A-1-013, Fig. 57A-1-014, Fig. 57A-1-015, Fig. 57A-1-016, Fig. 57A-1-017, Fig. 57A-1-018.	
	Effect of p: Fig. 57A-1-019, Fig. 57A-1-020, Fig. 57A-1-021, Fig. 57A-1-022; see also	92Mro
	Effect of γ-ray irradiation and substitution of chlorine by iodine: see	95Mro
	Dielectric anomaly appears around 170 K, which is considered as an over-critical phenomenon of an isomorphous transition between two ferroelectric states.	92Iwa, 97Car
b	Nonlinear dielectric properties: see	90Cac
c	Spontaneous polarization: Fig. 57A-1-023, Fig. 57A-1-024; see also	90Cac, 90Mro, 94Ram
	Coercive field: Fig. 57A-1-025.	
6a	Heat capacity: Fig. 57A-1-026; see also	94Ram, 94Str, 95Str
	Transition enthalpy and entropy: $\Delta H_{II-I} = 3.06 \cdot 10^3$ J mol^{-1}, $\Delta S_{II-I} = 10.6$ J K^{-1} mol^{-1}.	94Iwa
	Excess enthalpy and entropy estimated from a broad hump around 160 K in heat capacity: $\Delta H = 1.57 \cdot 10^3$ J mol^{-1}, $\Delta S = 9.85$ J K^{-1} mol^{-1}.	94Iwa
8a	Elastic stiffness: Fig. 57A-1-027.	
9a	Refractive indices: $n_a = 1.643(60)$, $n_b = 1.627(60)$, $n_c = 1.646(60)$ for $\lambda = 632.8$ nm at $T = 295$ K.	91Min
	Birefringence: Fig. 57A-1-028, Fig. 57A-1-029; see also	91Prz
	Far-infrared reflectivity spectra: see	93Mar
	Absorption in visible and ultraviolet region: see	91Min
b	Electrooptic effect: Fig. 57A-1-030; see also	91Min
d	Optical activity: see	94Prz
e	SHG: see	94Prz
10a	Raman scattering: no soft mode was observed in the vicinity of Θ_{II-I}.	93Kuo
	Raman scattering spectra: see	92Car, 93Kuo
	Raman scattering frequency shift: Fig. 57A-1-031, Fig. 57A-1-032.	
13a	NMR: Fig. 57A-1-033, Fig. 57A-1-034, Fig. 57A-1-035, Fig. 57A-1-036, Fig. 57A-1-037, Fig. 57A-1-038, Fig. 57A-1-039.	
15a	Domain structure: see	91Sze, 95Fra
b	Effect of electric field: see	91Pol
16	No ferroelastic domain was observed in the temperature range from 300 K to 80 K by polarizing microscope.	92Iwa

Table 57A-1-001. $(CH_3NH_3)_5Bi_2Cl_{11}$. Fractional coordinates [$\cdot 10^{-4}$] and equivalent isotropic temperature parameters [$\cdot 10^{-3}$ Å^2] in phase I (T = 349 K) and phase II (T = 294 K) [91Lef1]. For disordered atoms, the two equilibrium positions are labeled by primed and unprimed atoms with the same numbering. See Table 57A-1-004 for occupancy probability. All disordered atoms in phase II and C(2), C(2′), N(3), C(3) in phase I were refined with isotropic temperature parameters. U_{eq} for other atoms was estimated by $U_{eq} = (\Sigma U_{ii})/3$, where U_{ii} is defined by Eq. (d) in Introduction.

	x	y	z	U_{eq}		x	y	z	U_{eq}
Phase I (349 K)					Phase II (294 K)				
Bi	–1622(1)	822(1)	1091(1)	47(1)	Bi(1)	–1696(1)	826(1)	1010	41(1)
Cl(1)	0	0	0	77(12)	Bi(2)	1570(1)	–811(1)	–1179(1)	44(1)
Cl(2)	–575(4)	2487(4)	1144(3)	72(8)	Cl(1)	–83(4)	40(6)	21(5)	66(6)
Cl(3)	–2637(4)	–858(4)	1046(3)	81(8)	Cl(12)	–674(3)	2521(3)	1096(3)	58(5)
Cl(4)	–2958(4)	1522(4)	2122(3)	104(8)	Cl(13)	–2701(4)	–836(3)	1157(4)	71(7)
Cl(5)	–558(4)	194(5)	2478(4)	97(9)	Cl(14)	–3007(4)	1554(4)	2147(3)	83(6)
Cl(6)	–2701(5)	1433(4)	–275(3)	102(9)	Cl(15)	–610(4)	291(4)	2490(4)	86(8)
N(1)	–857(18)	2679(16)	3222(11)	125(39)	Cl(16)	–2889(4)	1373(4)	–281(3)	82(7)
N(2)	1762(23)	1466(19)	932(21)	75(48)	Cl(22)	461(4)	–2404(4)	–1227(4)	74(7)
N(2)′	1850(38)	180(42)	1609(31)	92(91)	Cl(23)	2638(4)	886(3)	–937(4)	67(6)
N(3)	79(48)	4533(41)	403(50)	164(31)	Cl(24)	2944(4)	–1488(4)	–2109(4)	95(7)
C(1)	88(19)	2629(23)	3671(14)	107(48)	Cl(25)	541(4)	–97(4)	–2502(4)	84(7)
C(2)	1930(49)	801(46)	1627(30)	111(19)	Cl(26)	2534(4)	–1479(4)	294(4)	90(7)
C(2)′	2202(44)	1045(39)	1317(39)	60(20)	N(11)	–907(12)	2713(11)	3200(11)	83(25)
C(3)	124(42)	5172(46)	–324(37)	76(18)	N(21)	–884(16)	7605(17)	1692(18)	113(36)
					N(12)	1737(14)	1506(15)	893(14)	82(7)
					N(12)′	1810(57)	192(57)	1763(52)	50(24)
					N(22)	1792(32)	6445(29)	3958(23)	58(13)
					N(22)′	1778(23)	5249(26)	3459(18)	64(9)
					N(3)	–136(13)	4719(20)	399(17)	142(39)
					C(11)	120(16)	2572(18)	3690(13)	104(33)
					C(21)	88(15)	7774(20)	1350(15)	165(44)
					C(12)	1984(20)	823(21)	1661(18)	85(7)
					C(12)′	1348(95)	1127(65)	1954(85)	78(41)
					C(22)	2031(48)	5697(50)	3426(32)	73(14)
					C(22)′	2212(35)	6116(32)	3805(30)	72(11)
					C(3)	–20(18)	5390(18)	–232(21)	88(38)

Table 57A-1-002. $(CH_3NH_3)_5Bi_2Cl_{11}$. Interatomic distances [Å] and angles [°] in phase I (T = 349 K) and phase II (T = 294 K) [91Lef1].

	Phase I	Phase II	
		i = 1	i =2
Bi(i)–Cl(1)	2.937(1)	2.807(7)	3.063(7)
Bi(i)–Cl(i2)	2.706(5)	2.724(5)	2.657(5)
Bi(i)–Cl(i3)	2.704(5)	2.679(5)	2.777(4)
Bi(i)–Cl(i4)	2.553(5)	2.639(5)	2.469(5)
Bi(i)–Cl(i5)	2.699(5)	2.776(6)	2.628(6)
Bi(i)–Cl(i6)	2.675(5)	2.627(5)	2.748(6)
N(i1)–C(i1)	1.41(3)	1.54(3)	1.38(3)
N(i2)–C(i2)	1.44(4)	1.55(4)	1.37(8)
N(i2)′–C(i2)′	1.37(5)	1.47(13)	1.44(6)
N(3)–C(3)	1.44(5)	1.36(4)	
Cl(1)–Bi(i)–Cl(i2)	89.7(1)	90.5(2)	88.2(2)
Cl(1)–Bi(i)–Cl(i3)	89.6(1)	93.6(2)	86.1(2)
Cl(1)–Bi(i)–Cl(i4)	176.4(1)	171.0(2)	178.2(2)
Cl(1)–Bi(i)–Cl(i5)	87.6(1)	87.8(2)	87.9(2)
Cl(1)–Bi(i)–Cl(i6)	92.8(1)	98.2(2)	87.4(2)
Cl(i2)–Bi(i)–Cl(i3)	179.0(2)	172.4(1)	173.4(2)
Cl(i2)–Bi(i)–Cl(i4)	89.5(2)	86.6(1)	92.9(2)
Cl(i2)–Bi(i)–Cl(i5)	90.0(2)	87.2(2)	91.5(2)
Cl(i2)–Bi(i)–Cl(i6)	90.6(2)	93.8(2)	88.9(2)
Cl(i3)–Bi(i)–Cl(i4)	91.1(2)	88.3(2)	92.9(2)
Cl(i3)–Bi(i)–Cl(i5)	89.2(2)	86.6(2)	91.6(2)
Cl(i3)–Bi(i)–Cl(i6)	90.2(2)	91.9(2)	87.5(2)
Cl(i4)–Bi(i)–Cl(i5)	88.8(2)	83.5(2)	93.6(2)
Cl(i4)–Bi(i)–Cl(i6)	90.7(2)	90.6(2)	91.1(2)
Cl(i5)–Bi(i)–Cl(i6)	179.2(2)	173.9(2)	175.3(2)
Bi(1)–Cl(1)–Bi(2)	180.0	175.7(3)	

Table 57A-1-003. $(CH_3NH_3)_5Bi_2Cl_{11}$. Selected Cl…N distances [Å] in phase I (T = 349 K) and phase II (T = 294 K) [91Lef1].

Phase I (349 K)			
Cl(2)…N(1)	3.24(3)	Cl(4)…N(2′^{ii})	3.10(9)
Cl(3)…N(1^{i})	3.30(5)	Cl(6)…N(2′^{iii})	3.26(10)
	Cl(2)…N(3)	3.21(10)	

Symmetry code: (i) x, y – 1/2, 1/2 – z; (ii) x – 1/2, – y, 1/2– z; (iii) – x, – y, – z.

Phase II (249 K)			
Cl(12)…N(11)	3.26(3)	Cl(22)…N(21^{i})	3.26(4)
Cl(23)…N(11^{i})	3.26(4)	Cl(13)…N(21^{ii})	3.31(5)
Cl(23)…N(12)	3.17(4)	Cl(22)…N(22^{i})	3.22(7)
Cl(14)…N(12^{iii})	3.35(4)	Cl(24)…N(22^{iv})	3.35(7)
Cl(24)…N(12^{v})′	2.95(13)	Cl(14)…N(22^{iii})′	3.25(6)
Cl(15)…N(12)′	3.32(11)	Cl(1)…N(22^{i})′	3.27(6)
		Cl(16)…N(22^{i})′	3.32(7)
	Cl(25)…N(3^{i})	3.31(4)	
	Cl(12)…N(3)	3.34(5)	

Symmetry code: (i) – x, 1/2– y, z – 1/2; (ii) x, y – 1, z; (iii) x – 1/2, 1/2 – y, z; (iv) 1/2– x, y – 1, z – 1/2; (v) 1/2– x, y, z – 1/2.

Table 57A-1-004. $(CH_3NH_3)_5Bi_2Cl_{11}$. Characterization of the disorder of methylammonium cations [91Lef1]. The translation is the distance between the centers of the C–N bonds corresponding to the two equilibrium positions.

	Occupancy probability of unprimed atoms	Reorientational process	
		Rotation [°]	Translation [Å]
Phase I (349 K)			
Methylammonium (2)	0.60(5)	140	0.82(15)
Methylammonium (3)	0.50	180	0.51(19)
Phase II (294 K)			
Methylammonium (12)	0.84(3)	119	1.20(20)
Methylammonium (22)	0.40(6)	141	0.56(12)

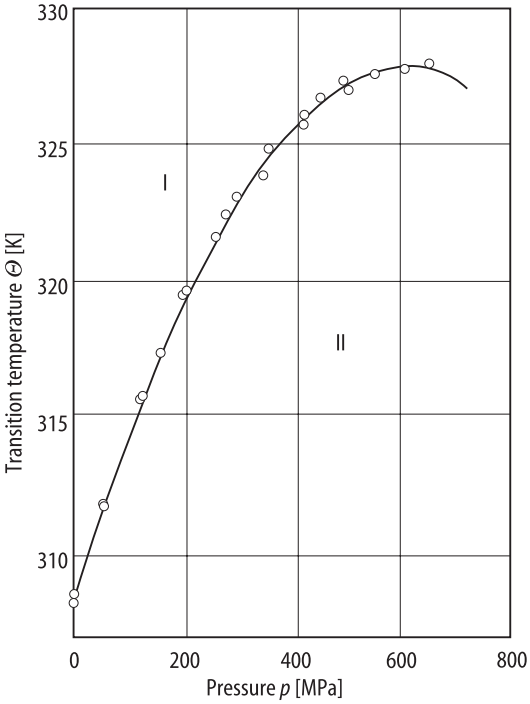

Fig. 57A-1-001. $(CH_3NH_3)_5Bi_2Cl_{11}$. Θ vs. p [95Ges].

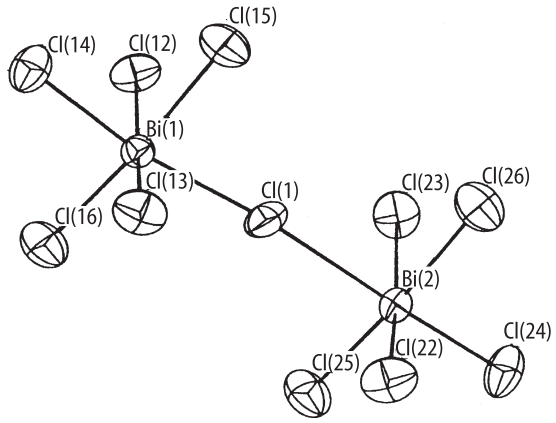

Fig. 57A-1-002. $(CH_3NH_3)_5Bi_2Cl_{11}$. The Bi_2Cl_{11} bioctahedra in phase II [91Lef1]. T = 294 K. The atom numbering follows Table 57A-1-001.

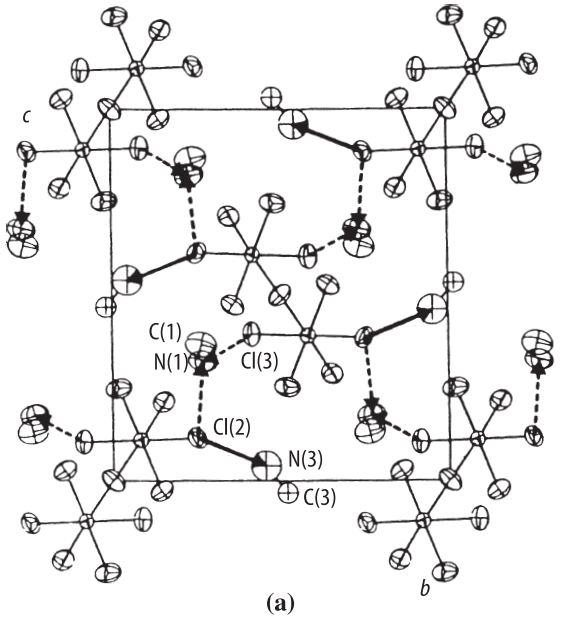

(a)

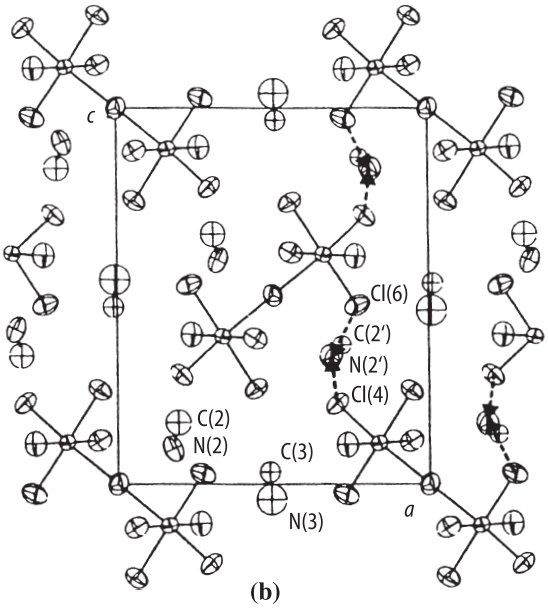

(b)

Fig. 57A-1-003. $(CH_3NH_3)_5Bi_2Cl_{11}$. Crystal structure of phase I at $T = 349$ K [91Lef1]. Projection along (**a**) [100] and (**b**) [010]. The dotted and double lines represent N…Cl hydrogen bonds from N(1) or N(2) and from N(3), respectively. Only atoms near the planes $x = 0$ for (a) and $y = 0$ for (b) are drawn.

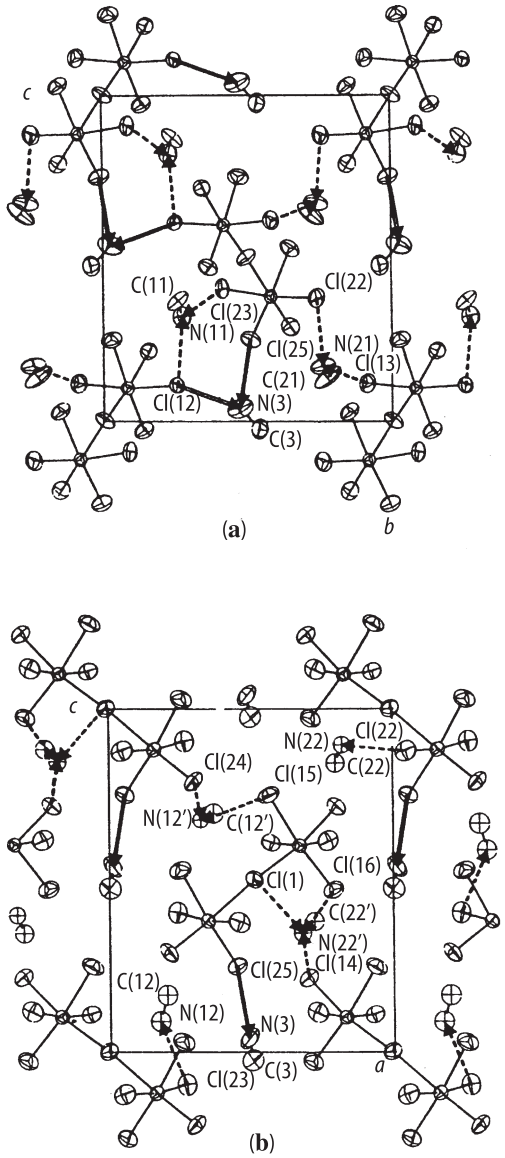

Fig. 57A-1-004. $(CH_3NH_3)_5Bi_2Cl_{11}$. Crystal structure of phase II at T = 294 K [91Lef1]. Projection along (**a**) [100] and (**b**) [010]. The dotted and double lines represent N…Cl hydrogen bonds from N(1) or N(2) and from N(3), respectively. Only atoms near the planes x = 0 for (a) and y = 0 for (b) are drawn. Note the different scales for (a) and (b).

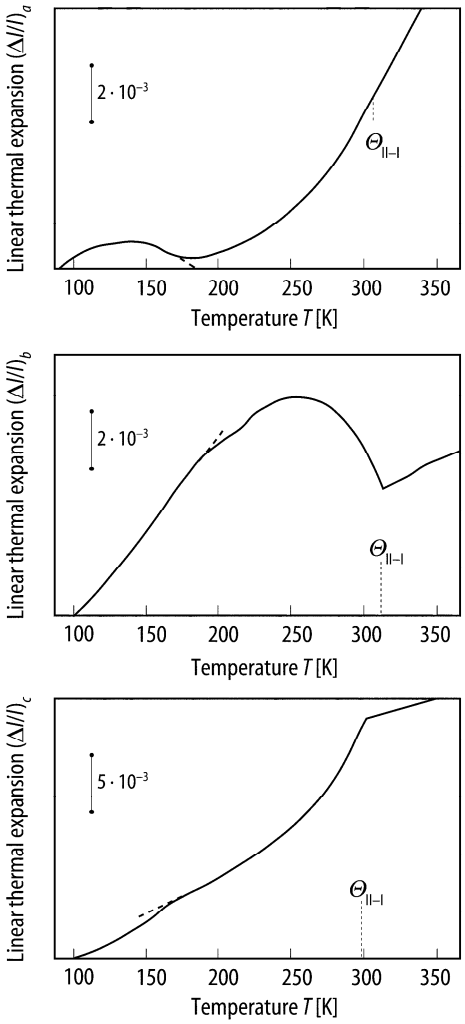

Fig. 57A-1-005. $(CH_3NH_3)_5Bi_2Cl_{11}$. $\Delta l/l$ vs. T [94Jak]. $(\Delta l/l)_a$, $(\Delta l/l)_b$, $(\Delta l/l)_c$: linear thermal expansion along a, b, and c axes, respectively.

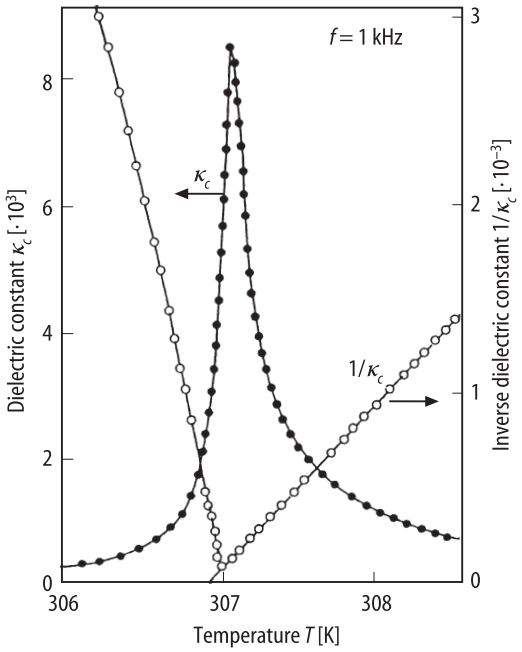

Fig. 57A-1-006. $(CH_3NH_3)_5Bi_2Cl_{11}$. κ_c, $1/\kappa_c$ vs. T [91Lef2]. f = 1 kHz.

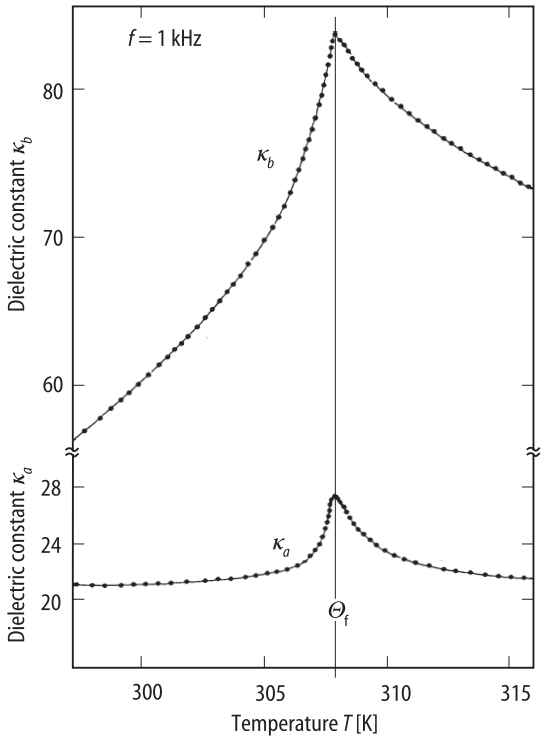

Fig. 57A-1-007. $(CH_3NH_3)_5Bi_2Cl_{11}$. κ_a, κ_b vs. T [91Lef2]. f = 1 kHz.

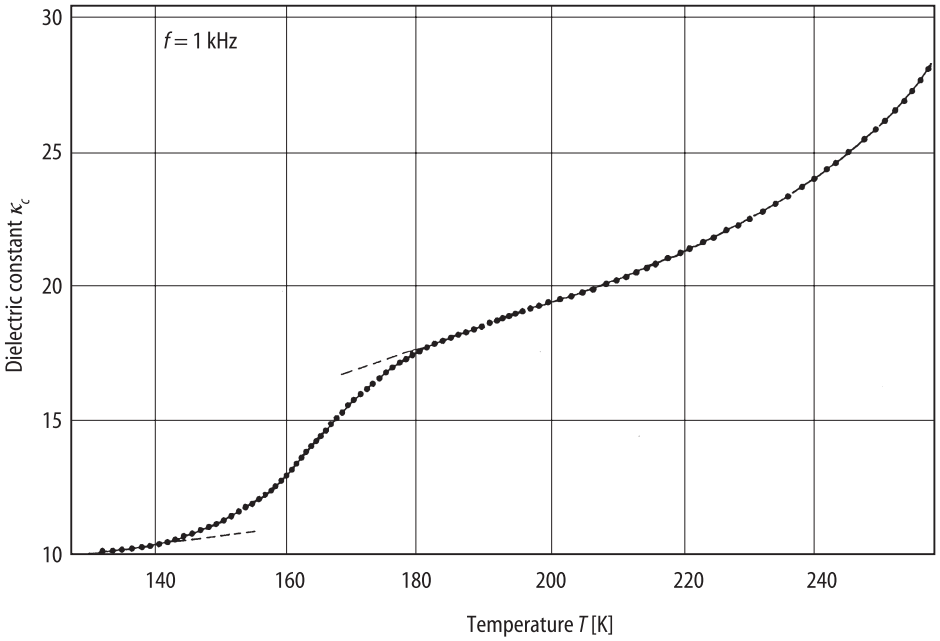

Fig. 57A-1-008. $(CH_3NH_3)_5Bi_2Cl_{11}$. κ_c vs. T in the low-temperature anomaly region [91Lef2]. f = 1 kHz.

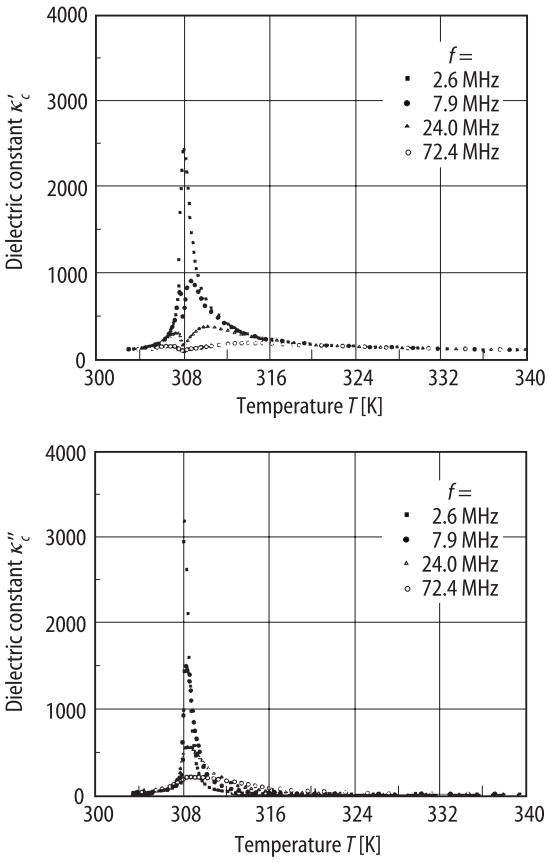

Fig. 57A-1-009. $(CH_3NH_3)_5Bi_2Cl_{11}$. κ_c', κ_c'' vs. T [90Iwa]. Parameter: f.

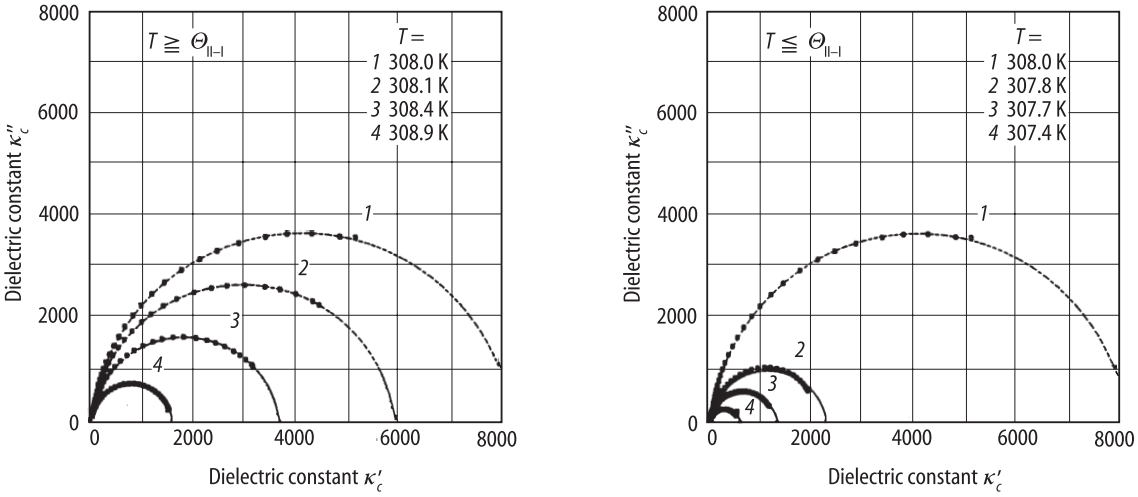

Fig. 57A-1-010. $(CH_3NH_3)_5Bi_2Cl_{11}$. Cole-Cole diagram of complex dielectric constant in the range of frequency from 1 MHz to 1 GHz [90Iwa]. Parameter: T. Θ_{II-I} = 308 K.

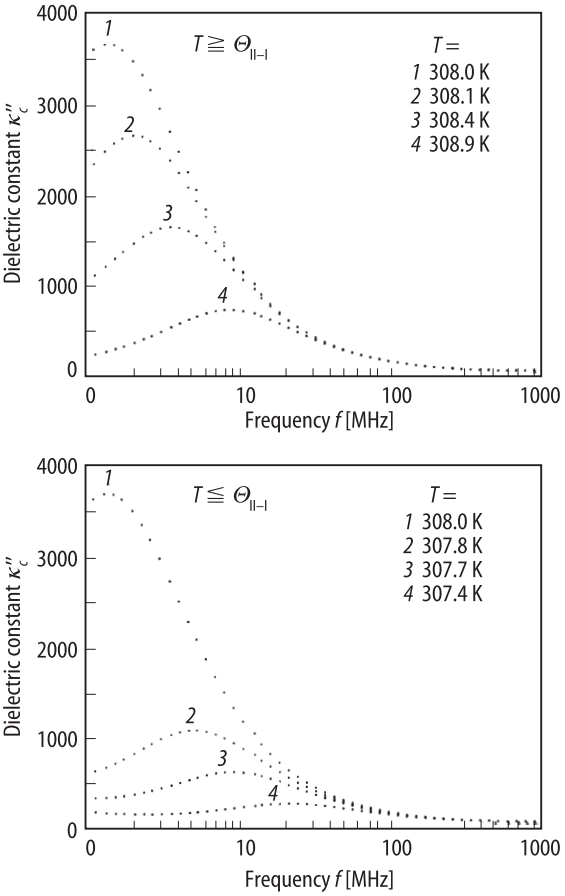

Fig. 57A-1-011. $(CH_3NH_3)_5Bi_2Cl_{11}$. κ_c'' vs. f [90Iwa]. Parameter: T. Θ_{II-I} = 308 K.

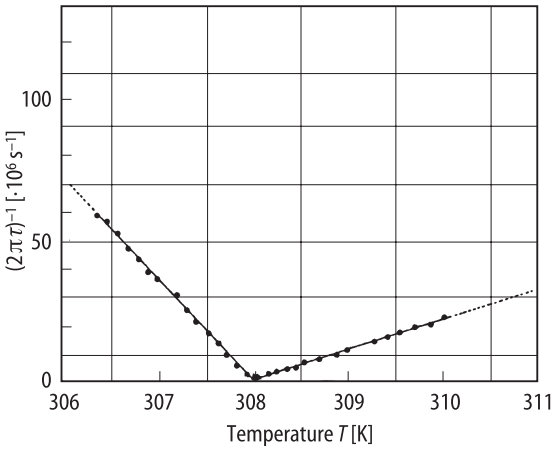

Fig. 57A-1-012. $(CH_3NH_3)_5Bi_2Cl_{11}$. $1/2\pi\tau$ vs. T [90Iwa]. τ: dielectric relaxation time.

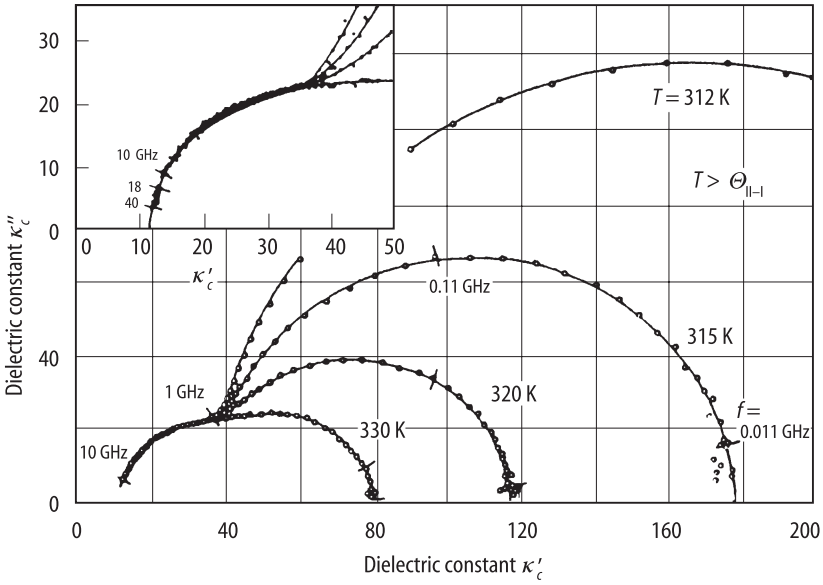

Fig. 57A-1-013. $(CH_3NH_3)_5Bi_2Cl_{11}$. Cole-Cole diagram of complex dielectric constant ($T > \Theta_{II-I}$) [92Paw]. Parameter: T. Θ_{II-I} = 308 K.

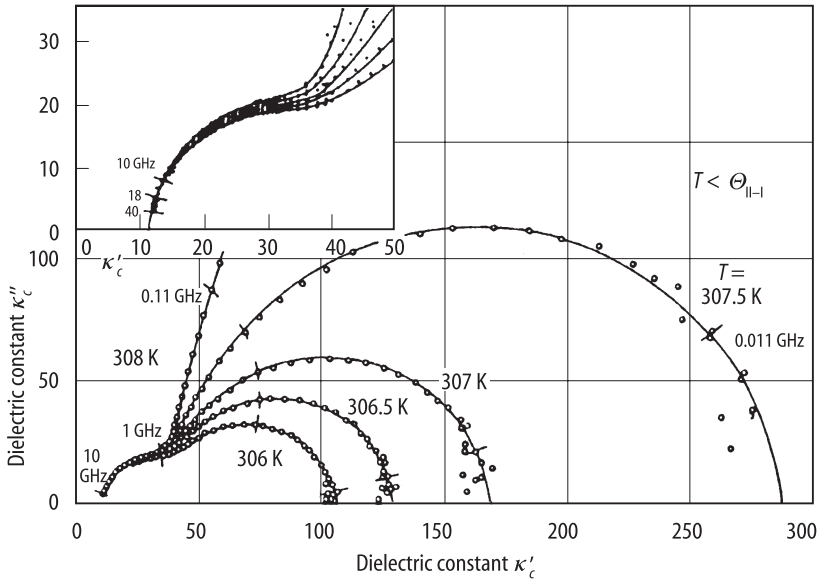

Fig. 57A-1-014. $(CH_3NH_3)_5Bi_2Cl_{11}$. Cole-Cole diagram of complex dielectric constant ($T < \Theta_{II-I}$) [92Paw]. Parameter: T. $\Theta_{II-I} = 308$ K.

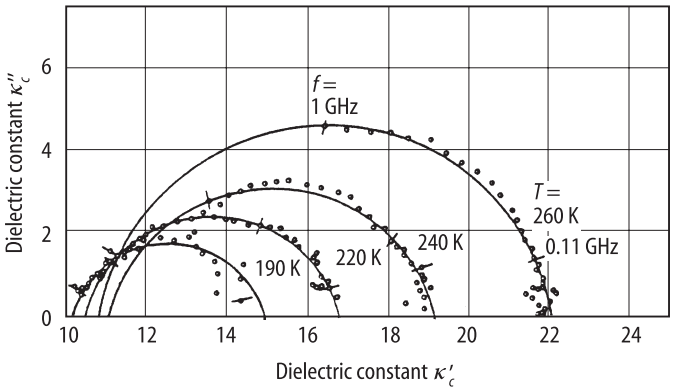

Fig. 57A-1-015. $(CH_3NH_3)_5Bi_2Cl_{11}$. Cole-Cole diagram of complex dielectric constant in phase II [92Paw]. Parameter: T.

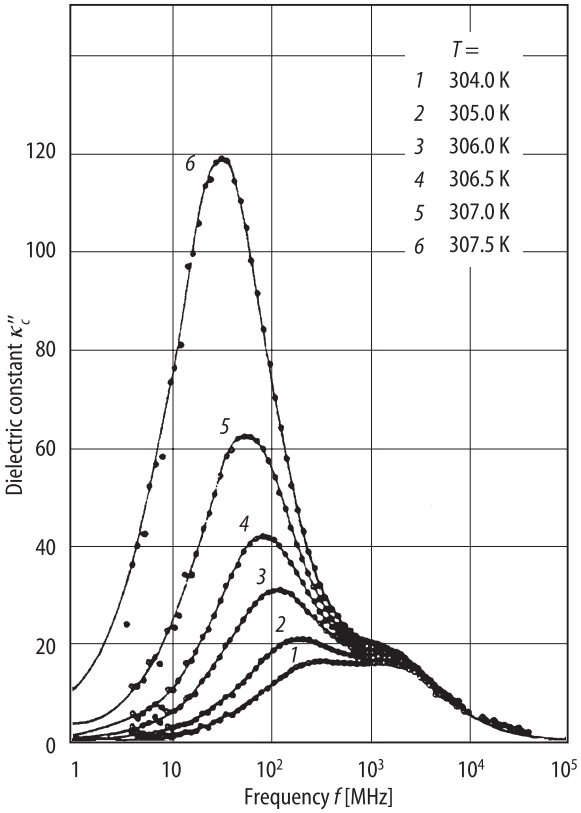

Fig. 57A-1-016. $(CH_3NH_3)_5Bi_2Cl_{11}$. κ_c'' vs. f [92Paw]. Parameter: T. Θ_{II-I} = 308 K.

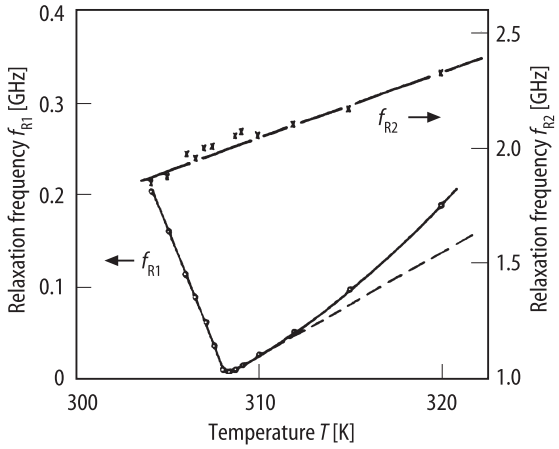

Fig. 57A-1-017. $(CH_3NH_3)_5Bi_2Cl_{11}$. f_{R1}, f_{R2} vs. T [92Paw]. f_{R1}, f_{R2}: relaxation frequencies of low-frequency and high-frequency dispersion.

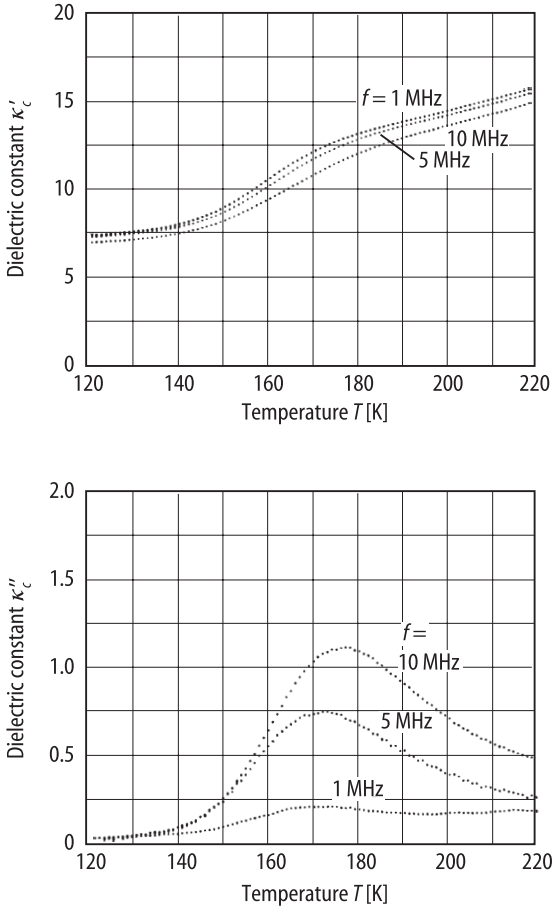

Fig. 57A-1-018. $(CH_3NH_3)_5Bi_2Cl_{11}$. κ_c', κ_c'' vs. T [92Iwa]. Parameter: f.

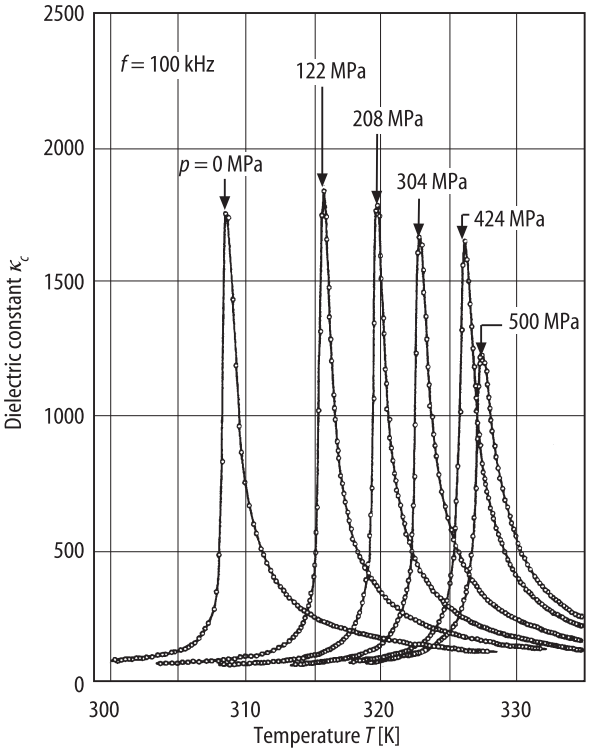

Fig. 57A-1-019. $(CH_3NH_3)_5Bi_2Cl_{11}$. κ_c vs. T [95Ges]. Parameter: p. f = 100 kHz.

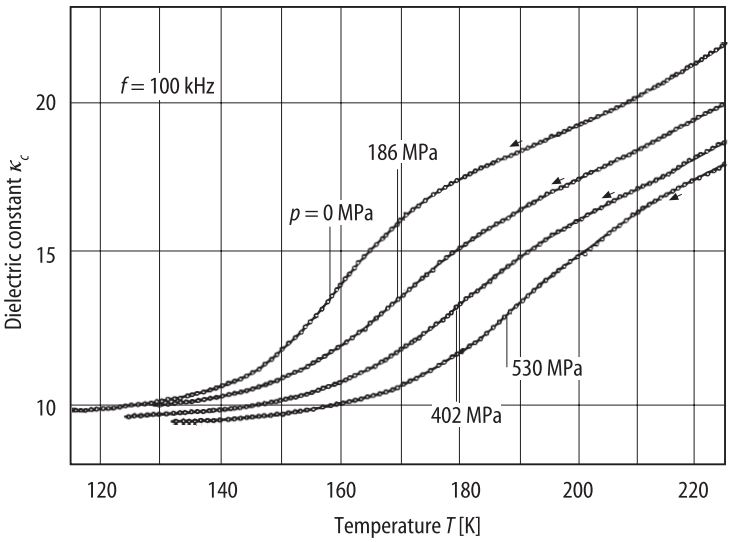

Fig. 57A-1-020. $(CH_3NH_3)_5Bi_2Cl_{11}$. κ_c vs. T [95Ges]. Parameter: p. f = 100 kHz.

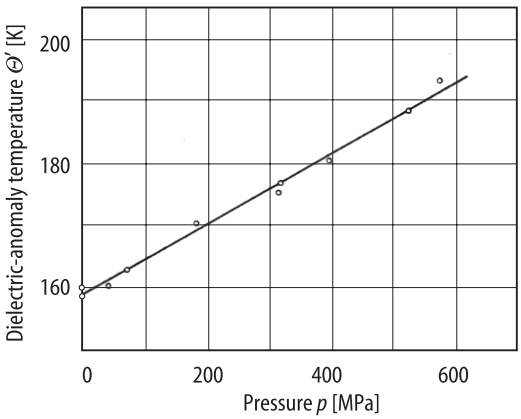

Fig. 57A-1-021. $(CH_3NH_3)_5Bi_2Cl_{11}$. Θ' vs. p [95Ges]. Θ': dielectric-anomaly temperature around 160 K, which is defined as the inflection point on κ_c vs. T curve (Fig. 57A-1-020).

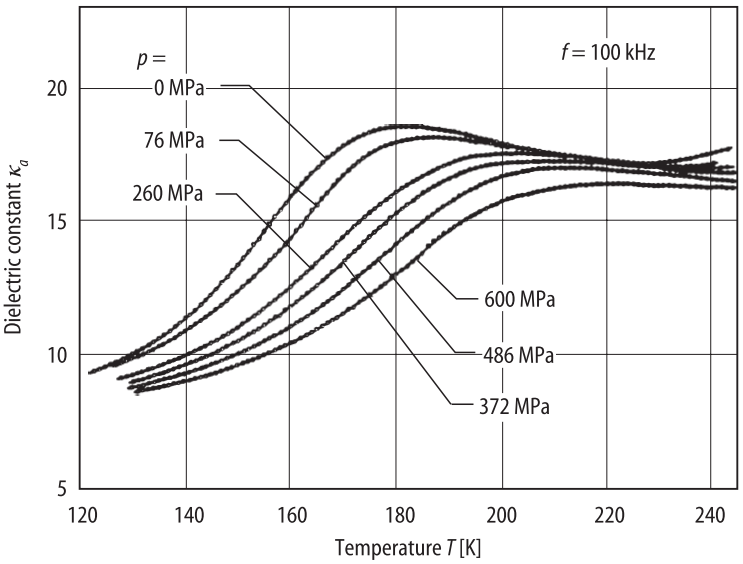

Fig. 57A-1-022. $(CH_3NH_3)_5Bi_2Cl_{11}$. κ_a vs. T [96Ges]. Parameter: p. f = 100 kHz.

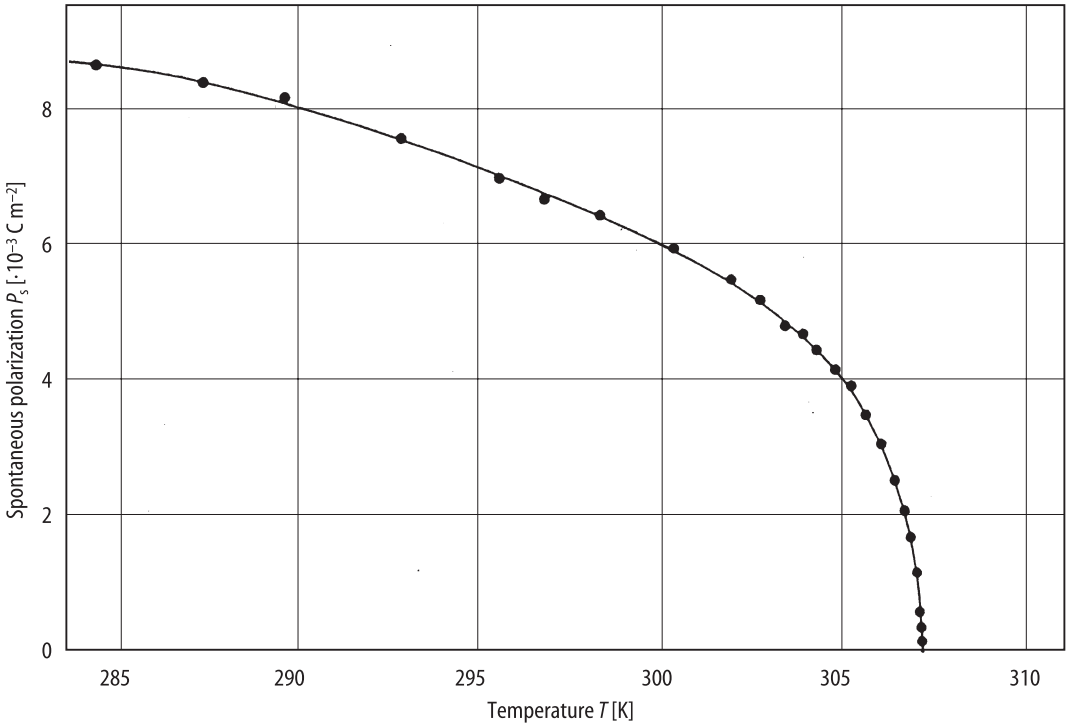

Fig. 57A-1-023. $(CH_3NH_3)_5Bi_2Cl_{11}$. P_s vs. T [91Lef2]. Sawyer-Tower method.

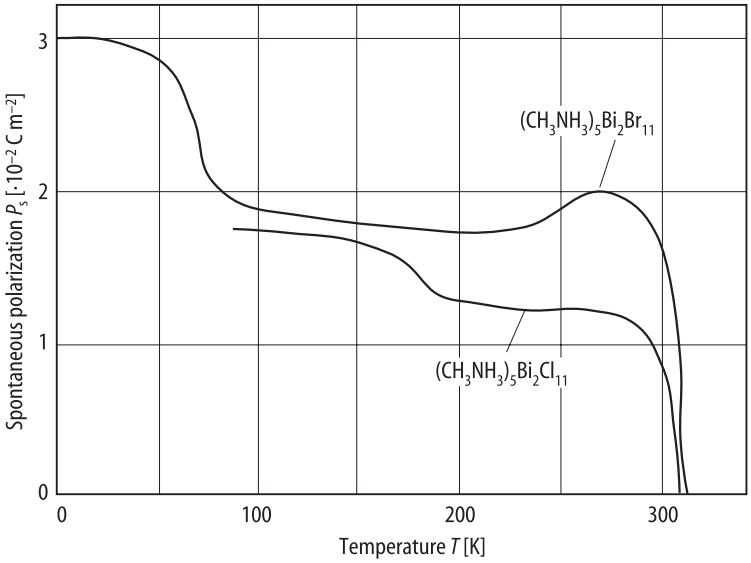

Fig. 57A-1-024. $(CH_3NH_3)_5Bi_2Cl_{11}$, $(CH_3NH_3)_5Bi_2Br_{11}$. P_s vs. T [91Mro]. Pyroelectric measurement.

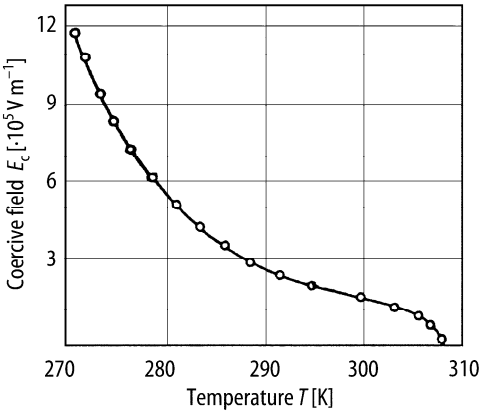

Fig. 57A-1-025. $(CH_3NH_3)_5Bi_2Cl_{11}$. E_c vs. T [90Mro]. Sawyer-Tower method.

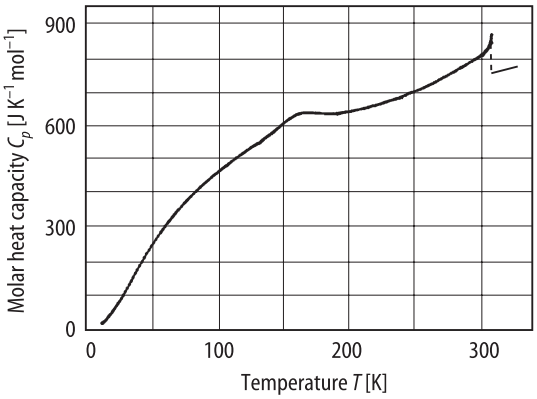

Fig. 57A-1-026. $(CH_3NH_3)_5Bi_2Cl_{11}$. C_p vs. T [94Iwa].

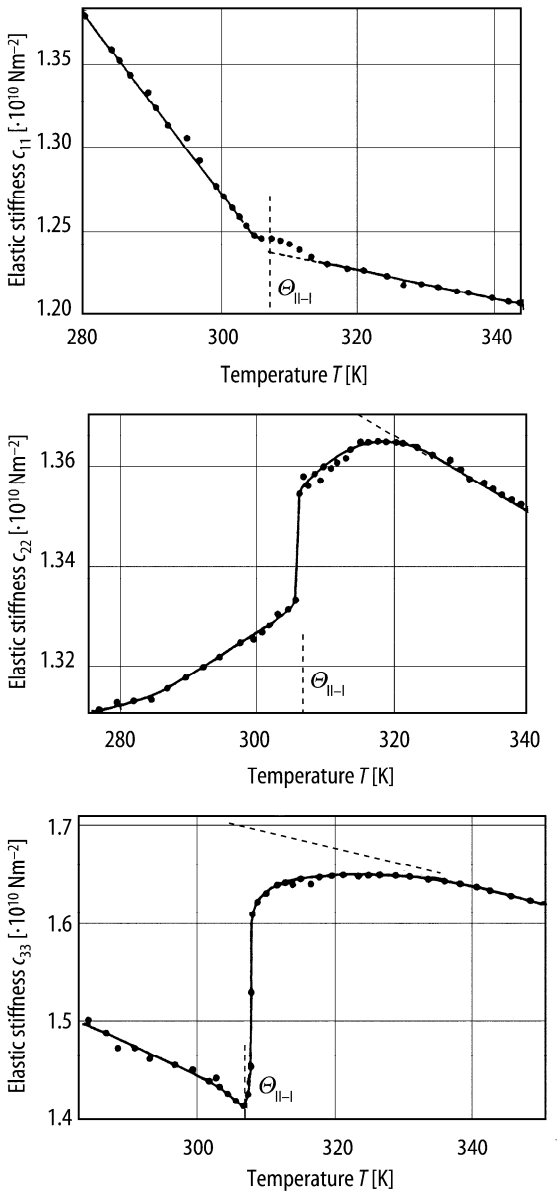

Fig. 57A-1-027. $(CH_3NH_3)_5Bi_2Cl_{11}$. c_{11}, c_{22}, c_{33} vs. T [92Jak]. c_{11}, c_{22}, c_{33}: elastic stiffness. Ultrasonic measurement at f = 1.5 MHz.

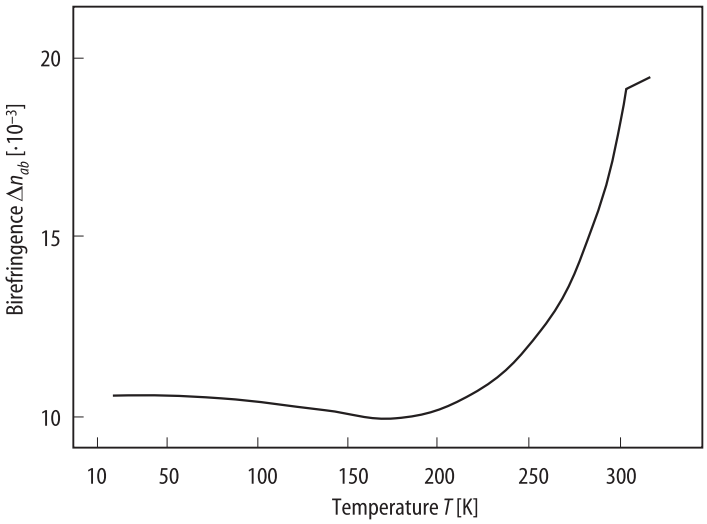

Fig. 57A-1-028. $(CH_3NH_3)_5Bi_2Cl_{11}$. Δn_{ab} vs. T [94Prz]. $\Delta n_{ab} = n_a - n_b$. $\lambda = 632.8$ nm.

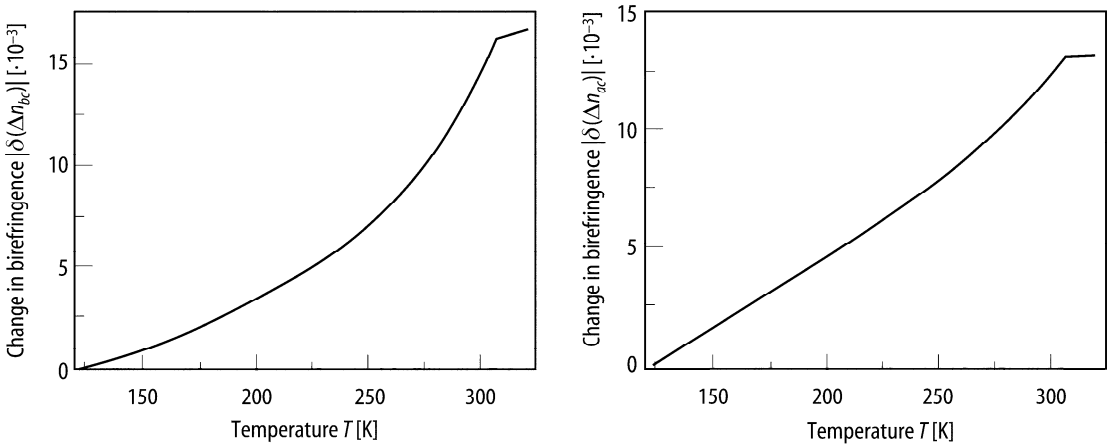

Fig. 57A-1-029. $(CH_3NH_3)_5Bi_2Cl_{11}$. $|\delta(\Delta n_{bc})|$, $|\delta(\Delta n_{ac})|$ vs. T [95Prz]. $\lambda = 632.8$ nm. $\delta(\Delta n_{bc})$, $\delta(\Delta n_{ac})$: change in birefringence in *bc* and *ac* planes.

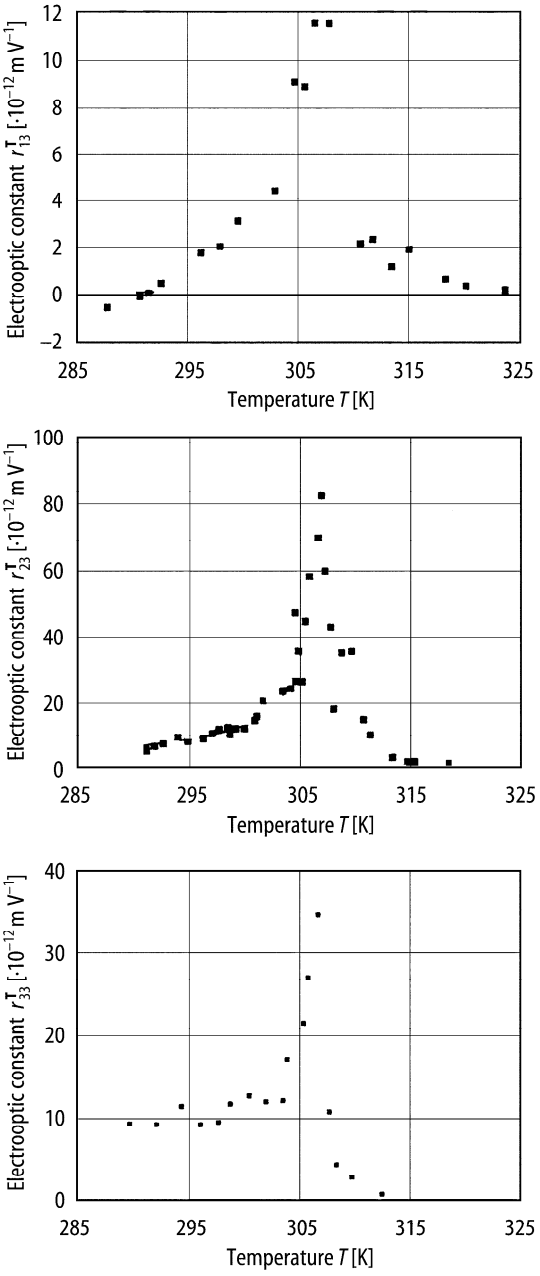

Fig. 57A-1-030. $(CH_3NH_3)_5Bi_2Cl_{11}$. $r_{13}^{\mathbf{T}}, r_{23}^{\mathbf{T}}, r_{33}^{\mathbf{T}}$ vs. T [95Min]. $r_{\lambda i}^{\mathbf{T}}$: electrooptic constant for $\boldsymbol{E}$ at stress $\mathbf{T} = 0$. $\lambda = 632.8$ nm.The crystal was driven with rectangular positive voltage pulses with $f = 10$ kHz.

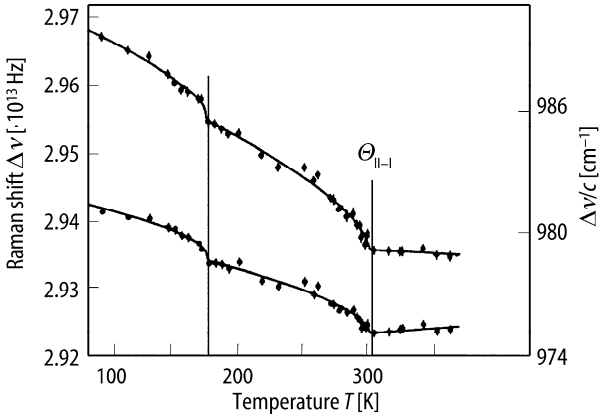

Fig. 57A-1-031. $(CH_3NH_3)_5Bi_2Cl_{11}$. $\Delta\nu$ vs. T [92Car]. $\Delta\nu$: Raman shift for the two components of the C–N stretching mode. See [92Car] for the mode assignment. Vertical lines indicate the temperatures of anomalous change in Raman shift.

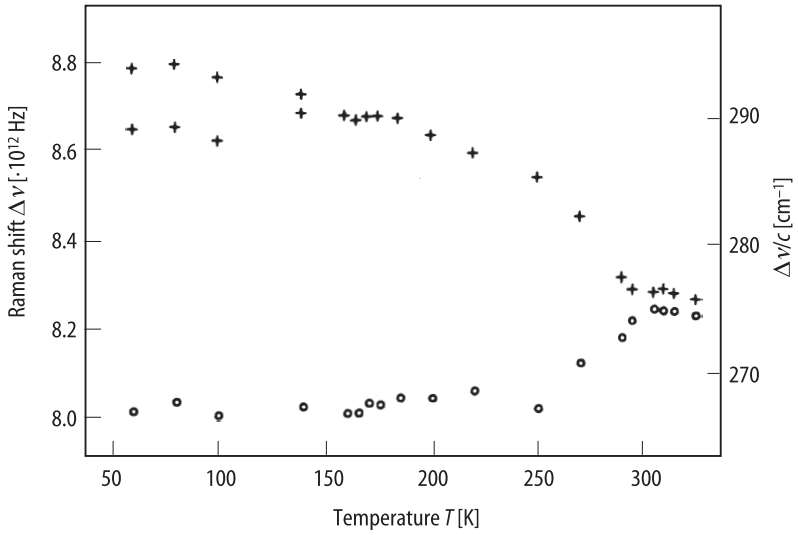

Fig. 57A-1-032. $(CH_3NH_3)_5Bi_2Cl_{11}$. $\Delta\nu$ vs. T [93Kuo]. $\Delta\nu$: Raman shift for the two components of $Bi_2Cl_{11}^{5-}$ anion stretching mode.

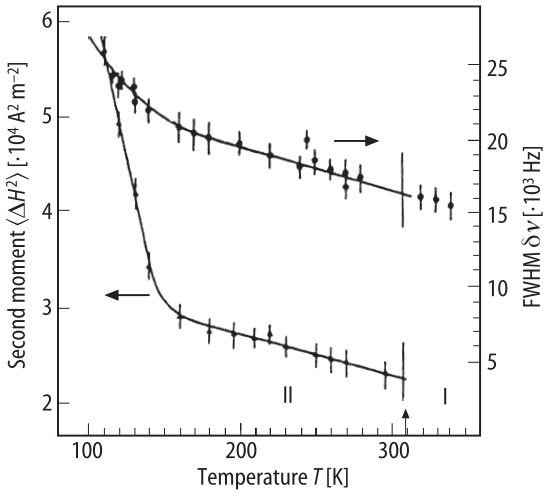

Fig. 57A-1-033. $(CH_3NH_3)_5Bi_2Cl_{11}$. $\langle \Delta H^2 \rangle$, $\delta\nu$ vs. T [94Dec]. $\langle \Delta H^2 \rangle$, $\delta\nu$: second moment and full width at half maximum of ^{1}H magnetic resonance curve.

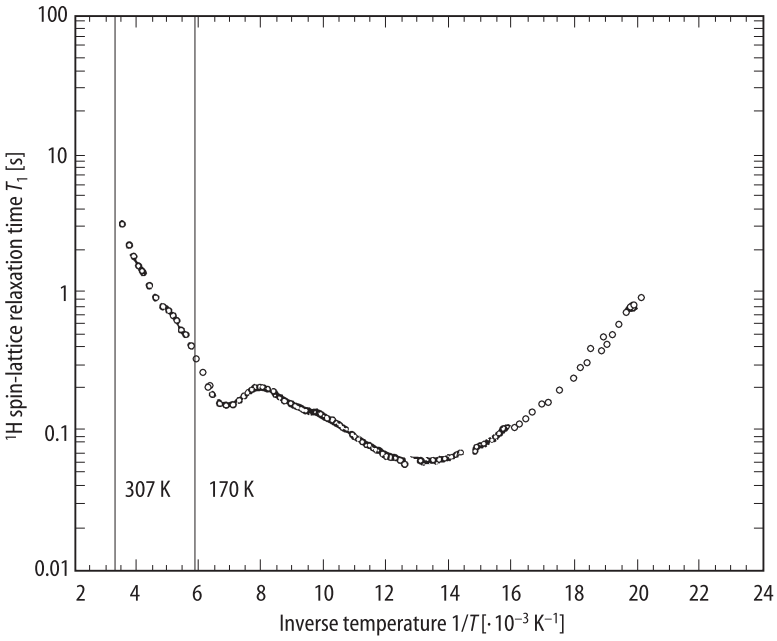

Fig. 57A-1-034. $(CH_3NH_3)_5Bi_2Cl_{11}$. T_1 vs. $1/T$ [93Med]. T_1: ^{1}H spin-lattice relaxation time. ν_L = 55.2 MHz.

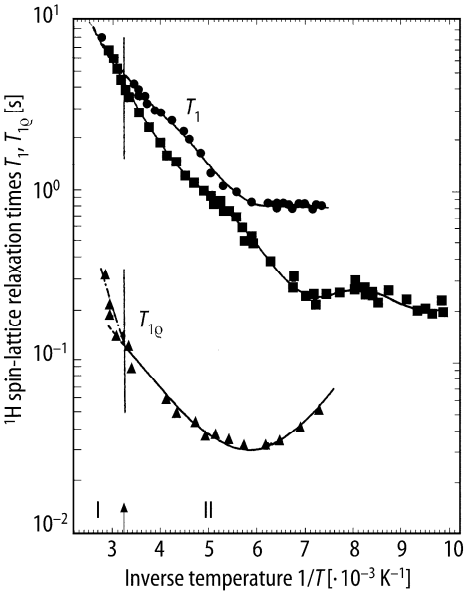

Fig. 57A-1-035. $(CH_3NH_3)_5Bi_2Cl_{11}$. T_1, $T_{1\rho}$ vs. $1/T$ [94Dec]. T_1: ^{1}H spin-lattice relaxation time at ν_L = 400 MHz (full circle) and 100 MHz (full square). $T_{1\rho}$: ^{1}H spin-lattice relaxation time in rotating frame, where $19 \cdot 10^3/4\pi$ A m^{-1} field pulse was employed.

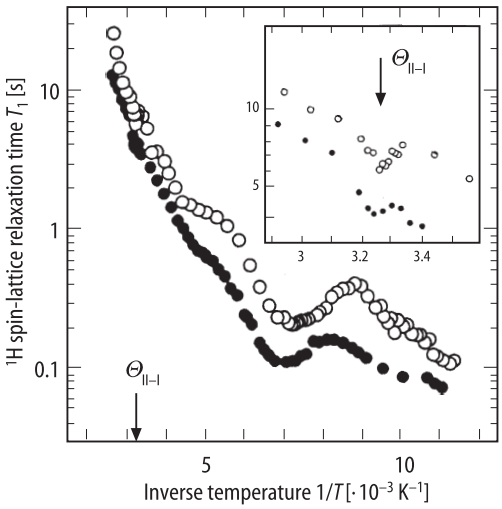

Fig. 57A-1-036. $(CH_3NH_3)_5Bi_2Cl_{11}$, $(CH_3ND_3)_5Bi_2Cl_{11}$. T_1 vs. $1/T$ [95Ish]. T_1: ^{1}H spin-lattice relaxation time of $(CH_3NH_3)_5Bi_2Cl_{11}$ (full circle) and $(CH_3ND_3)_5Bi_2Cl_{11}$ (open circle). ν_L = 40.8 MHz. Θ_{II-I} for $(CH_3ND_3)_5Bi_2Cl_{11}$ is shown by arrow.

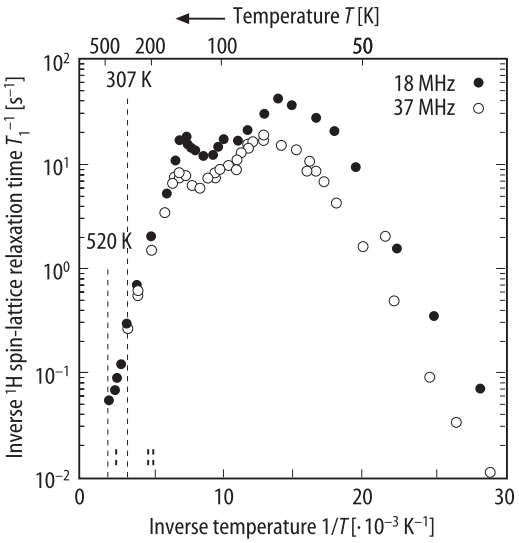

Fig. 57A-1-037. $(CH_3NH_3)_5Bi_2Cl_{11}$. T_1^{-1} vs. $1/T$ [95Nag]. T_1: ^1H spin-lattice relaxation time for ν_L = 18 MHz (full circle) and 37 MHz (open circle).

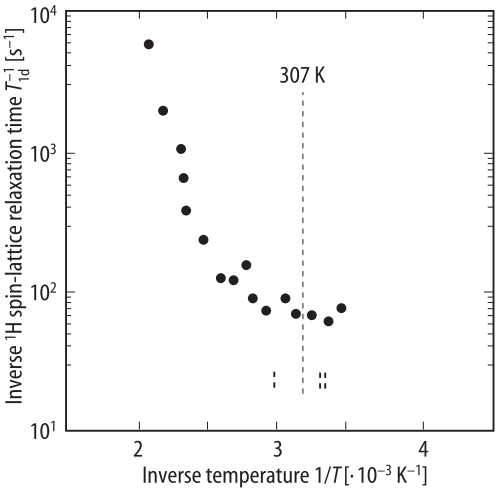

Fig. 57A-1-038. $(CH_3NH_3)_5Bi_2Cl_{11}$. T_{1d}^{-1} vs. $1/T$ [95Nag]. T_{1d}: ^1H spin-lattice relaxation time in dipolar field. ν_L = 37 MHz.

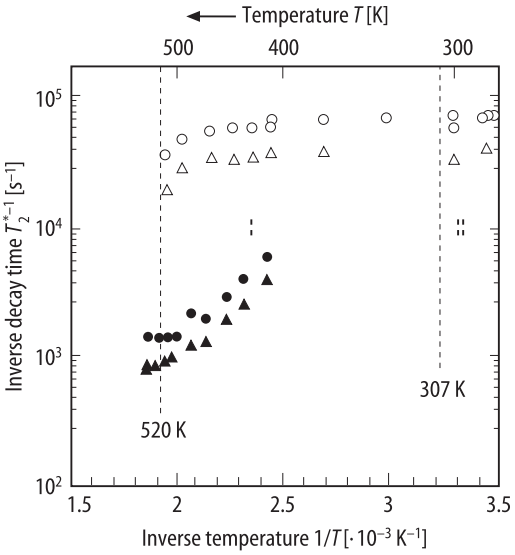

Fig. 57A-1-039. $(CH_3NH_3)_5Bi_2Cl_{11}$. T_2^{*-1} vs. $1/T$ [95Nag]. T_2^* : the decay time of the transverse magnetization of ^1H to a half (open circle, full circle), and to a quarter (open triangle, full triangle). Open circle and open triangle were obtained on heating. Full circle and full triangle were obtained on cooling and their low values indicate that cation-diffusing phase was supercooled to about $T = 400$ K.

References

89Jak Jakubas, R., Sobczyk, L., Lefebvre, J.: Ferroelectrics **100** (1989) 143.
90Cac Cach, R., Jakubas, R.: Ferroelectrics **108** (1990) 121.
90Iwa Iwata, M., Ishibashi, Y.: J. Phys. Soc. Jpn. **59** (1990) 4239.
90Mro Mróz, J., Jakubas, R.: Ferroelectrics Lett. **11** (1990) 53.
91Lef1 Lefebvre, J., Carpentier, P., Jakubas, R.: Acta Crystallogr. Sect. B **47** (1991) 228.
91Lef2 Lefebvre, J., Carpentier, P., Jakubas, R., Sobczyk, L.: Phase Transitions **33** (1991) 31.
91Min Miniewicz, A., Jakubas, R.: J. Mol. Electron. **7** (1991) 55.
91Mro Mróz, J., Jakubas, R.: Ferroelectrics **118** (1991) 29.
91Pol Polomska, M., Jakubas, R.: Izv. Akad. Nauk SSSR, Ser. Fiz. **55** (1991) 545; Bull. Acad. Sci. USSR, Phys. Ser. (English Transl.) **55** (1991) 126.
91Prz Przeslawski, I., Kosturek, B., Jakubas, R.: Izv. Akad. Nauk SSSR, Ser. Fiz. **55** (1991) 510; Bull. Acad. Sci. USSR, Phys. Ser. (English Transl.) **55** (1991) 89.
91Pyk Pykacz, H., Jakubas, R.: Acta Phys. Pol. A **79** (1991) 695.
91Sze Szezesniak, L., Meyer, K.-P., Jakubas, R.: Izv. Akad. Nauk SSSR, Ser. Fiz. **55** (1991) 543; Bull. Acad. Sci. USSR, Phys. Ser. (English Transl.) **55** (1991) 123.
92Car Carpentier, P., Lefebvre, J., Jakubas, R.: J. Phys. Condens. Matter **4** (1992) 2985.
92Iwa Iwata, M., Ishibashi, Y.: J. Phys. Soc. Jpn. **61** (1992) 4615.
92Jak Jakubas, R., Lefebvre, J., Fontaine, H., François, P.: Solid State Commun. **81** (1992) 515.
92Mro Mróz, J., Poprawski, R., Jakubas, R.: Pol. J. Chem. **66** (1992) 827.
92Paw Pawlaczyk, C., Jakubas, R., Planta, K., Bruch, C., Unruh, H.-G.: J. Phys. Condens. Matter **4** (1992) 2695.
93Kuo Kuok, M.H., Ng, S.C., Iwata, M., Ishibashi, Y.: Solid State Commun. **86** (1993) 151.
93Mar Marqueton, Y., Miniewicz, A., Jakubas, R.: Ferroelectrics **145** (1993) 109.
93Med Medycki, W., Piślewski, N., Jakubas, R.: Solid State Nucl. Magn. Reson. **2** (1993) 197.
94Dec Decressain, R., Cochon, E., Lefebvre, J., Meurer, B., Jakubas, R.: J. Phys. Chem. Solids **55** (1994) 139.
94Iwa Iwata, M., Tojo, T., Atake, T., Ishibashi, Y.: J. Phys. Soc. Jpn. **63** (1994) 3751.
94Jak Jakubas, R., François, P., Lefebvre, J.: Acta Phys. Pol. A **85** (1994) 579.
94Prz Przesławski, J., Kosturek, B., Jakubas, R., Lingard, R., Arzt, S., Fitzmaurice, A.: Ferroelectrics **152** (1994) 367.
94Ram Ramos, S., Del Cerro, J., Pawlowski, A., Jakubas, R.: Ferroelectrics **159** (1994) 173.
94Str Strukov, B.A., Poprawski, R., Taraskin, S.A., Mróz, J.: Phys. Status Solidi (a) **143** (1994) K9.
95Car Carpentier, P., Lefebvre, J., Jakubas, R.: Acta Crystallogr. Sect. B **51** (1995) 167.
95Fra Franke, K., Weihnacht, M.: Ferroelectrics Lett. **19** (1995) 25.
95Ges Gesi, K., Iwata, M., Ishibashi, Y.: J. Phys. Soc. Jpn. **64** (1995) 2650.
95Ish Ishimaru, S., Suzuki, K., Ikeda, R.: J. Phys. Soc. Jpn. **64** (1995) 1754.
95Min Miniewicz, A., Żuk, W., Jakubas, R.: Ferroelectrics **165** (1995) 241.
95Mro Mróz, J., Pykacz, H., Jakubas, R.: Acta Phys. Pol. A **88** (1995) 369.
95Nag Nagatomo, S., Takeda, S., Yamaguchi, K., Iwata, M., Ishibashi, Y.: J. Phys. Soc. Jpn. **64** (1995) 391.
95Prz Przesławski, J.: J. Phys. Condens. Matter **7** (1995) 4169.
95Str Strukov, B.A., Poprawski, R., Taraskin, S.A., Pavlov, S.V., Mroz, J.: Ferroelectrics **168** (1995) 61.
96Ges Gesi, K., Iwata, M., Ishibashi, Y.: J. Phys. Soc. Jpn. **65** (1996) 14.
97Car Carpentier, P., Zieliński, P., Lefebvre, J., Jakubas, R.: Z. Phys. B **102** (1997) 403.

No. 57A-2 $(CH_3NH_3)_5Bi_2Br_{11}$, Pentakis(methylammonium) undecabromodibismuthate

(M = 1457.23)

1a Ferroelectricity in $(CH_3NH_3)_5Bi_2Br_{11}$ was discovered by Jakubas et al. in 1989. 89Jak1

b

phase	III [a])	II	I	89Jak1
state	F [a])	F	P	[a]) 89Mro
crystal system		orthorhombic		
space group		$Pca2_1 - C_{2v}^5$ [b])		[b]) 90Mat
Θ [K]	77 [a])		312.1	

P_s || [001]. 89Jak1
$\rho_X = 3.119 \cdot 10^3$ kg m^{-3} at T = 297 K. 90Mat
Phase diagram in regard to p: Fig. 57A-2-001; see also 90Mro
$d\Theta_{II-I}/dp = 0.060$ K MPa^{-1}. 95Ges

2a Crystal growth:
1: $(CH_3NH_3)_5Bi_2Br_{11}$ was synthesized by a reaction of $Bi(OH)_3$ and CH_3NH_3Br in 40% HBr. Single crystals were grown from a dilute HBr solution by slow evaporation at 290 K. 89Jak1
2: Single crystals were grown by a slow evaporation of an aqueous solution of CH_3NH_3Br and $(BiO)_2CO_3$ with a small excess of HBr. 89Mro
3: $(CH_3NH_3)_5Bi_2Br_{11}$ was synthesized in aqueous solution of CH_3NH_3Br and $BiBr_3$ with a great excess of HBr. Single crystals were grown by slowly cooling aqueous solution from about 100 °C to 30 °C. 90Iwa

3a Unit cell parameters: a = 13.405(3) Å, b = 14.462(3) Å, c = 16.006(3) Å at T = 297 K. 90Mat
b Z = 4 in phase II. 89Jak1
Positional and temperature parameters: Table 57A-2-001.
Interatomic distances and angles: Table 57A-2-002, Table 57A-2-003.
Crystal structure: Fig. 57A-2-002, Fig. 57A-2-003.

4 Thermal expansion: Fig. 57A-2-004, Fig. 57A-2-005; see also 89Jak2

5a Dielectric constant around Θ_{II-I}: Fig. 57A-2-006, Fig. 57A-2-007; see also 90Paw, 91Min
Dielectric constant around Θ_{III-II}: Fig. 57A-2-008, Fig. 57A-2-009; see also 89Mro
Curie-Weiss constant: see 89Jak1, 90Iwa, 91Min
Dielectric dispersion: Fig. 57A-2-010, Fig. 57A-2-011, Fig. 57A-2-012, Fig. 57A-2-013, Fig. 57A-2-014, Fig. 57A-2-015, Fig. 57A-2-016, Fig. 57A-2-017, Fig. 57A-2-018, Fig. 57A-2-019.
Effect of p: Fig. 57A-2-020; see also 90Mro
Effect of γ-ray irradiation: see 95Mro
b Effect of E_{bias}: see 90Cac, 92Orz
c Spontaneous polarization: Fig. 57A-2-021, Fig. 57A-2-022; see also 90Cac, 91Min
Coercive field: Fig. 57A-2-023; see also 92Pyk

6a Heat capacity: Fig. 57A-2-024, Fig. 57A-2-025; see also 92Paw2
Transition enthalpy and entropy: 92Str
$\Delta H_{II-I} = 5.14(20) \cdot 10^3$ J mol^{-1}, $\Delta S_{II-I} = 17.7$ J K^{-1} mol^{-1}.

8a	Elastic stiffness: Table 57A-2-004; Fig. 57A-2-026.	
9a	Refractive indices:	
	$n_a = 1.984$, $n_b = 1.956$, $n_c = 1.977$ for $\lambda = 488$ nm at RT;	93Pav
	$n_a = 1.908(70)$, $n_b = 1.887(70)$, $n_c = 1.915(70)$ for $\lambda = 632.8$ nm at 290 K.	95Min
	Fig. 57A-2-027.	
	Birefringence: Fig. 57A-2-028, Fig. 57A-2-029.	
	Far-infrared reflectivity spectra: see	93Mar
	Infrared absorption: see	90Bha
	Absorption in visible region: Fig. 57A-2-030.	
b	Electrooptic constants:	
	$r_{13}^{\mathbf{T}} = 2.7(5) \cdot 10^{-12}$, $r_{23}^{\mathbf{T}} = -5.7(9) \cdot 10^{-12}$, $r_{33}^{\mathbf{T}} = 9.0(9) \cdot 10^{-12}$ m V^{-1} at $T = 295$ K for	95Min
	$\lambda = 632.8$ nm when the crystal is driven with rectangular positive voltage pulses at $f = 10$ kHz.	
	Fig. 57A-2-031; see also	90Min
d	Optical activity: see	94Prz
e	SHG: see	94Prz
10a	Raman scattering: no soft mode was observed in the vicinity of Θ_{II-I}, see	90Jak, 90Bha
b	Brillouin scattering: Fig. 57A-2-032.	
13a	NMR: Fig. 57A-2-033.	
15a	Domain structure: see	89Pol
	Domain dynamics: see	90Pol, 91Pol, 91Sze, 94Mat, 95Mat
16	Internal bias field: see	92Pyk

Table 57A-2-001. $(CH_3NH_3)_5Bi_2Br_{11}$. Fractional coordinates and isotropic temperature parameters [$Å^2$] in phase II at T = 297 K [90Mat]. Anisotropic temperature parameters were used for Bi and Br atoms in analysis, and values of $B_{eq} = \Sigma B_{ii}/3$ are given for the atoms with B_{ii} defined by Eq. (a) in Introduction.

Atom	x	y	z	B_{eq} or B
Bi(1)	0.8443(1)	0.3322(1)	0.31	2.11(8)
Bi(2)	0.1676(1)	0.1660(1)	0.0833(1)	1.66(7)
Br(1)	0.0095(4)	0.2459(7)	0.2008(6)	4.3(2)
Br(11)	0.7343(4)	0.1594(4)	0.2962(5)	3.8(3)
Br(12)	0.9636(4)	0.4909(5)	0.3220(5)	5.3(3)
Br(13)	0.7102(5)	0.4012(6)	0.4196(5)	5.3(4)
Br(14)	0.9541(5)	0.2568(6)	0.4535(5)	5.2(4)
Br(15)	0.7485(6)	0.4021(5)	0.1724(5)	5.7(4)
Br(21)	0.2692(4)	0.3363(4)	0.0773(5)	4.3(3)
Br(22)	0.0610(4)	0.9933(4)	0.0913(4)	3.5(2)
Br(23)	0.2985(4)	0.0867(5)	0.9776(5)	3.5(3)
Br(24)	0.0516(5)	0.2227(6)	0.9488(4)	5.3(4)
Br(25)	0.2849(5)	0.1094(5)	0.2268(5)	4.5(3)
N(11)	–0.013(6)	0.517(5)	0.071(5)	11.4(21)
C(11)	0.043(7)	0.430(6)	0.053(6)	15.2(34)
C(12)	0.224(5)	0.365(4)	0.313(4)	7.6(16)
N(12)	0.189(3)	0.283(3)	0.361(3)	5.3(10)
N(13)	1.007(3)	0.772(4)	0.171(3)	5.4(12)
C(13)	0.998(5)	0.724(5)	0.253(4)	7.2(19)
N(21)	1.087(2)	0.981(3)	0.882(2)	3.7(8)
C(21)	0.990(3)	0.980(3)	0.836(3)	3.1(10)
C(22)	0.283(3)	0.823(3)	0.055(3)	4.0(11)
N(22)	0.328(2)	0.900(2)	0.103(2)	3.3(7)

Table 57A-2-002. $(CH_3NH_3)_5Bi_2Br_{11}$. Interatomic distances [Å] and angles [°] in the complex anion in phase II at $T = 297$ K [90Mat].

Interatomic distances [Å]			
Bi(1)–Br(1)	3.085(8)	Bi(2)–Br(1)	3.060(8)
Bi(1)–Br(11)	2.910(6)	Bi(2)–Br(21)	2.816(6)
Bi(1)–Br(12)	2.804(7)	Bi(2)–Br(22)	2.880(6)
Bi(1)–Br(13)	2.703(8)	Bi(2)–Br(23)	2.694(7)
Bi(1)–Br(14)	2.938(8)	Bi(2)–Br(24)	2.779(7)
Bi(1)–Br(15)	2.743(8)	Bi(2)–Br(25)	2.901(8)

Bond angles [°]			
Br(1)–Bi(1)–Br(11)	88.5(2)	Br(1)–Bi(2)–Br(21)	91.5(2)
Br(1)–Bi(1)–Br(12)	87.7(2)	Br(1)–Bi(2)–Br(22)	87.5(2)
Br(1)–Bi(1)–Br(13)	174.0(2)	Br(1)–Bi(2)–Br(23)	176.3(2)
Br(1)–Bi(1)–Br(14)	86.2(2)	Br(1)–Bi(2)–Br(24)	88.7(2)
Br(1)–Bi(1)–Br(15)	91.7(2)	Br(1)–Bi(2)–Br(25)	89.7(2)
Br(11)–Bi(1)–Br(12)	175.7(2)	Br(21)–Bi(2)–Br(22)	179.0(2)
Br(11)–Bi(1)–Br(13)	91.7(2)	Br(21)–Bi(2)–Br(23)	92.1(2)
Br(11)–Bi(1)–Br(14)	89.7(2)	Br(21)–Bi(2)–Br(24)	89.2(2)
Br(11)–Bi(1)–Br(15)	91.1(2)	Br(21)–Bi(2)–Br(25)	90.7(2)
Br(12)–Bi(1)–Br(13)	91.9(2)	Br(22)–Bi(2)–Br(23)	89.0(2)
Br(12)–Bi(1)–Br(14)	88.0(2)	Br(22)–Bi(2)–Br(24)	90.7(2)
Br(12)–Bi(1)–Br(15)	91.2(2)	Br(22)–Bi(2)–Br(25)	89.4(2)
Br(13)–Bi(1)–Br(14)	88.9(2)	Br(23)–Bi(2)–Br(24)	90.2(2)
Br(13)–Bi(1)–Br(15)	94.2(2)	Br(23)–Bi(2)–Br(25)	91.4(2)
Br(14)–Bi(1)–Br(15)	177.8(2)	Br(24)–Bi(2)–Br(25)	178.4(2)
Bi(1)–Br(1)–Bi(2)	176.5(3)		

Table 57A-2-003. $(CH_3NH_3)_5Bi_2Br_{11}$. Selected N...Br distances [Å] in phase II at $T = 297$ K [90Mat].

N(11)...Br(21^{i})	3.61(8)	N(21)...Br(11^{vi})	3.43(4)
N(12)...Br(14^{ii})	3.50(4)	N(21)...Br(22^{vii})	3.37(3)
N(12)...Br(21^{iii})	3.59(4)	N(21)...Br(23^{viii})	3.57(3)
N(12)...Br(23^{iv})	3.40(5)	N(22)...Br(22^{ix})	3.48(3)
N(13)...Br(14^{v})	3.55(5)	N(22)...Br(23^{x})	3.39(3)
N(13)...Br(22)	3.52(6)	N(22)...Br(25^{viii})	3.66(3)

Symmetry code:

(i) $-1/2+x, 1-y, z$;
(ii) $-1+x, y, z$;
(iii) $1/2-x, y, 1/2+z$;
(iv) $1/2-x, y, -1/2+z$;
(v) $1-x, 1-y, -1/2+z$;
(vi) $1-x, 1-y, 1/2+z$;
(vii) $x, y, 1+z$;
(viii) $x, 1+y, z$;
(ix) $1/2+x, 2-y, z$;
(x) $x, 1+y, -1+z$.

Table 57A-2-004. $(CH_3NH_3)_5Bi_2Br_{11}$. $c_{\lambda\mu}$ [$\cdot 10^9$ Nm^{-2}] at RT [93Pav]. Determined by Brillouin scattering. $\lambda = 488$ nm.

c_{11}	c_{22}	c_{33}	c_{44}	c_{55}	c_{66}	c_{12}	c_{23}	c_{13}
14.69	14.81	18.19	3.26	2.69	2.88	8.07	8.58	8.76

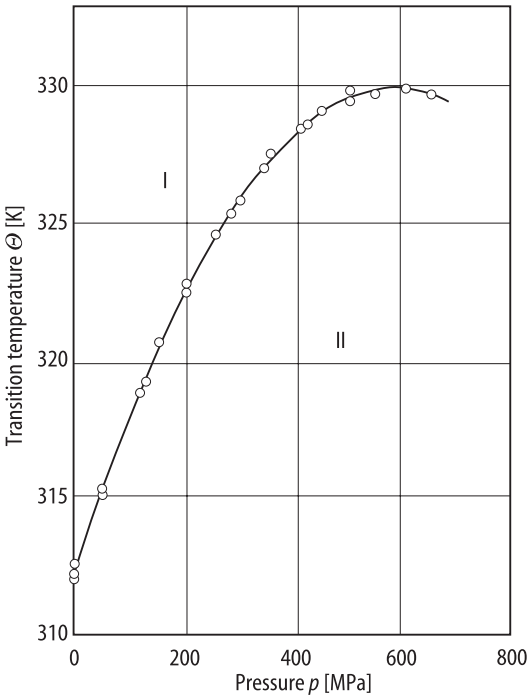

Fig. 57A-2-001. $(CH_3NH_3)_5Bi_2Br_{11}$. Θ vs. p [95Ges].

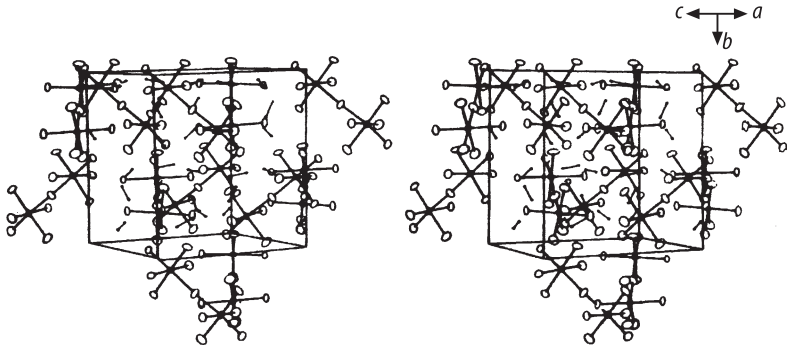

Fig. 57A-2-002. $(CH_3NH_3)_5Bi_2Br_{11}$. Stereoscopic view of unit-cell packing of the crystal structure in phase II at T = 297 K [90Mat]. Filled ellipsoids correspond to Bi atoms; solid-line contoured ellipsoids represent Br atoms; discrete vectors show C–N bond axes in methylammonium cations.

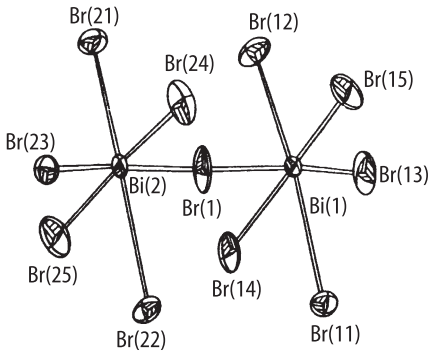

Fig. 57A-2-003. $(CH_3NH_3)_5Bi_2Br_{11}$. The $Bi_2Br_{11}^{5-}$ anion [90Mat]. The atom numbering scheme follows Table 57A-2-001.

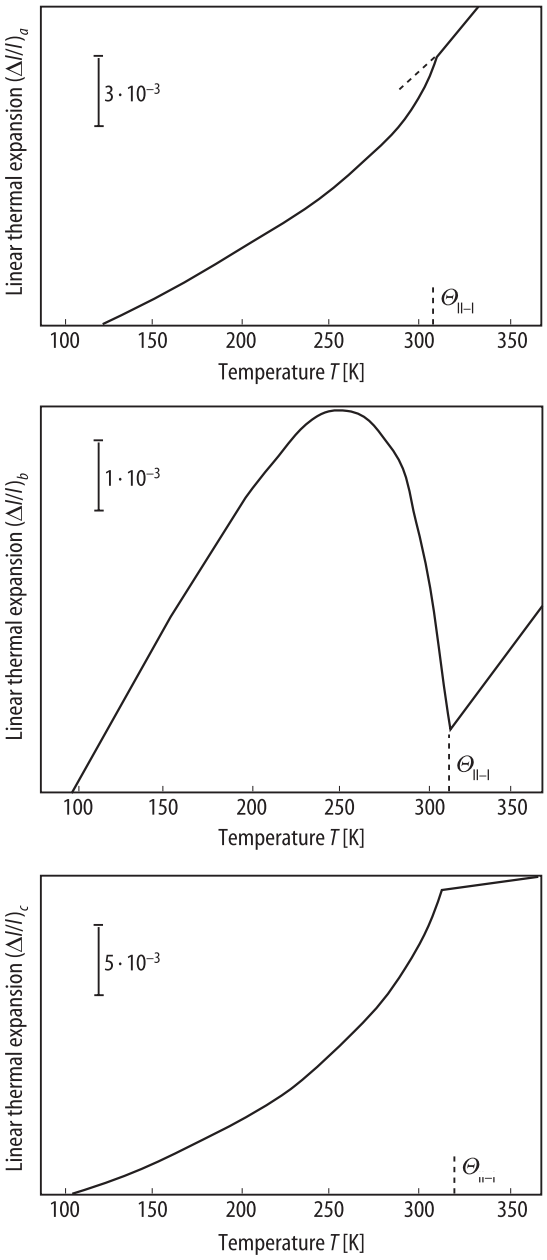

Fig. 57A-2-004. $(CH_3NH_3)_5Bi_2Br_{11}$. $\Delta l/l$ vs. T [94Jak]. $(\Delta l/l)_a$, $(\Delta l/l)_b$, $(\Delta l/l)_c$: linear thermal expansion along a, b and c axis, respectively.

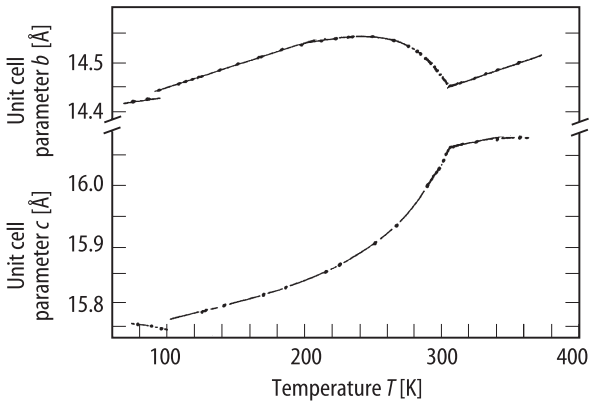

Fig. 57A-2-005. $(CH_3NH_3)_5Bi_2Br_{11}$. *b*, *c* vs. *T* [95Tom]. *b*, *c*: unit cell parameters.

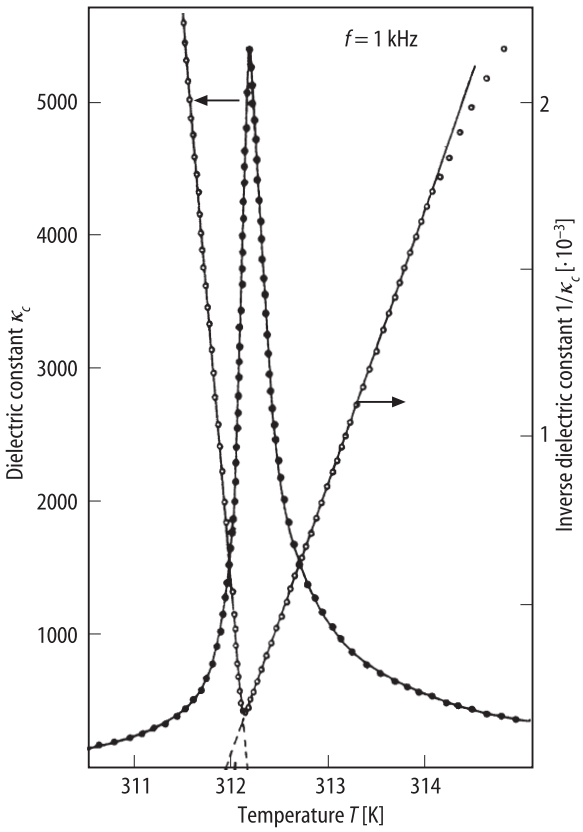

Fig. 57A-2-006. $(CH_3NH_3)_5Bi_2Br_{11}$. κ_c, $1/\kappa_c$ vs. *T* [89Jak3]. *f* = 1 kHz.

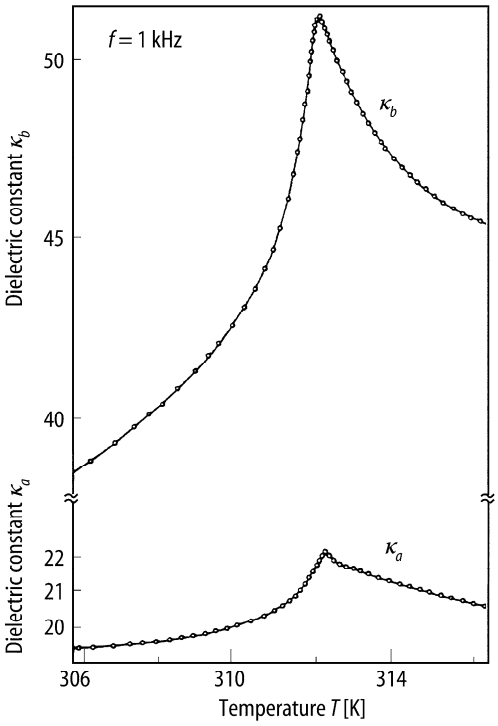

Fig. 57A-2-007. $(CH_3NH_3)_5Bi_2Br_{11}$. κ_a, κ_b vs. T [89Jak1]. f = 1 kHz. On heating.

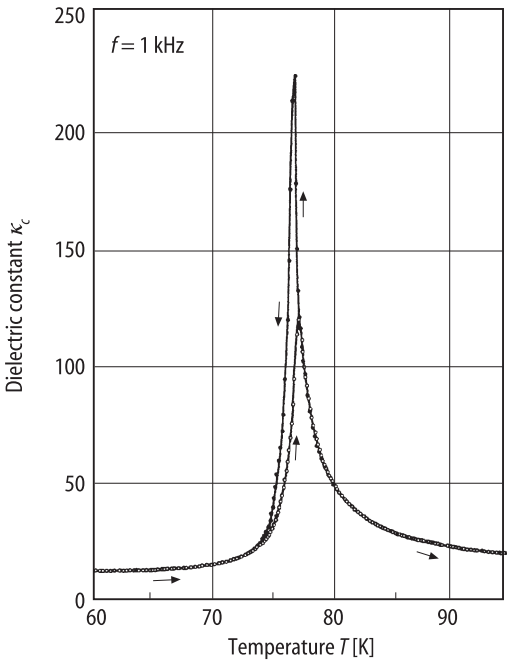

Fig. 57A-2-008. $(CH_3NH_3)_5Bi_2Br_{11}$. κ_c vs. T [96Ges]. f = 1 kHz.

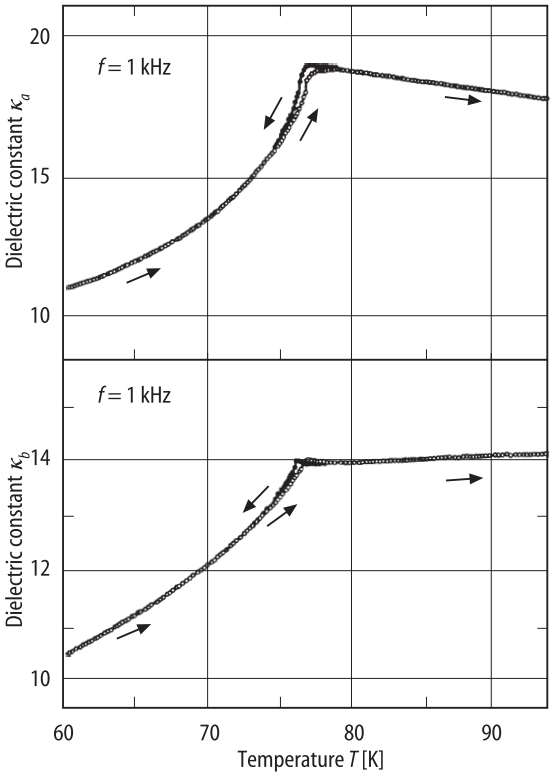

Fig. 57A-2-009. $(CH_3NH_3)_5Bi_2Br_{11}$. κ_a, κ_b vs. T [96Ges]. f = 1 kHz.

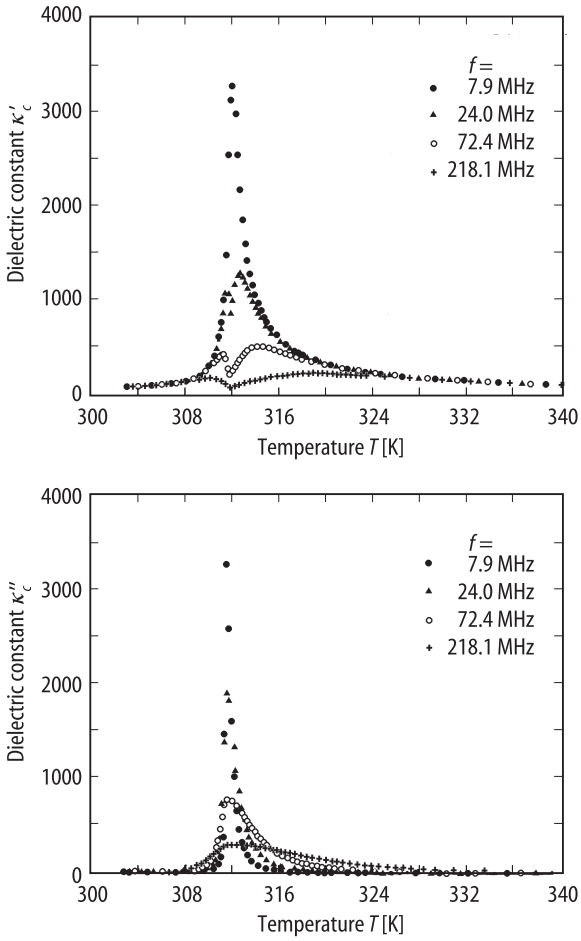

Fig. 57A-2-010. $(CH_3NH_3)_5Bi_2Br_{11}$. κ_c', κ_c'' vs. T [90Iwa]. Parameter: f.

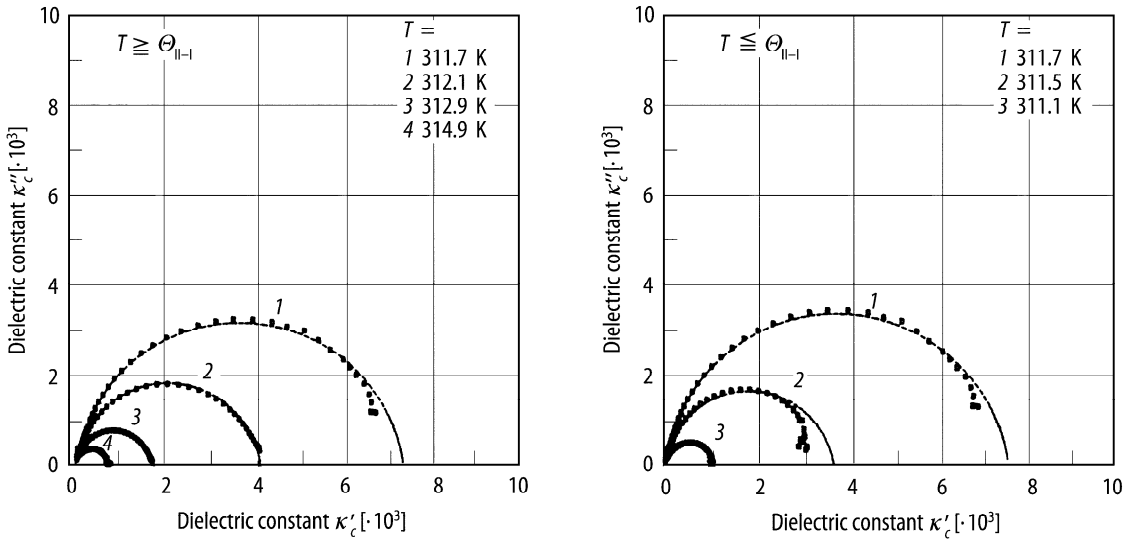

Fig. 57A-2-011. $(CH_3NH_3)_5Bi_2Br_{11}$. Cole-Cole diagram of complex dielectric constant in the range of frequency from 1 MHz to 1 GHz [90Iwa]. Parameter: T. Θ_{II-I} = 311.7 K.

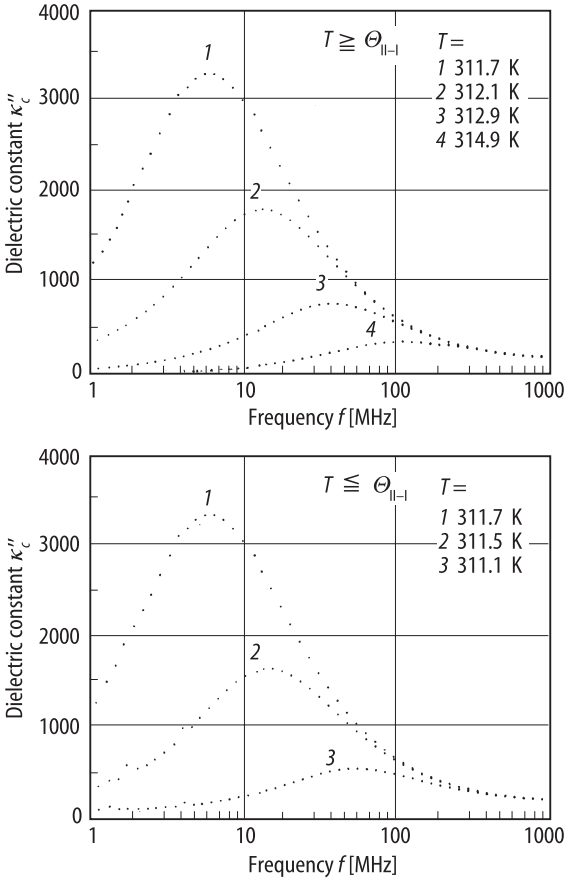

Fig. 57A-2-012. $(CH_3NH_3)_5Bi_2Br_{11}$. κ_c'' vs. f [90Iwa]. Parameter: T. Θ_{II-I} = 311.7 K.

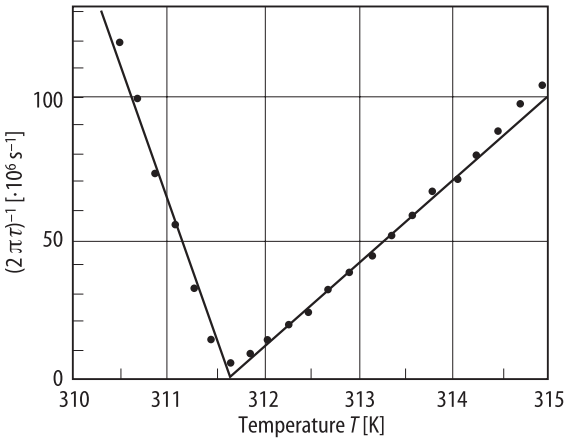

Fig. 57A-2-013. $(CH_3NH_3)_5Bi_2Br_{11}$. $1/2\pi\tau$ vs. T [90Iwa]. τ: dielectric relaxation time.

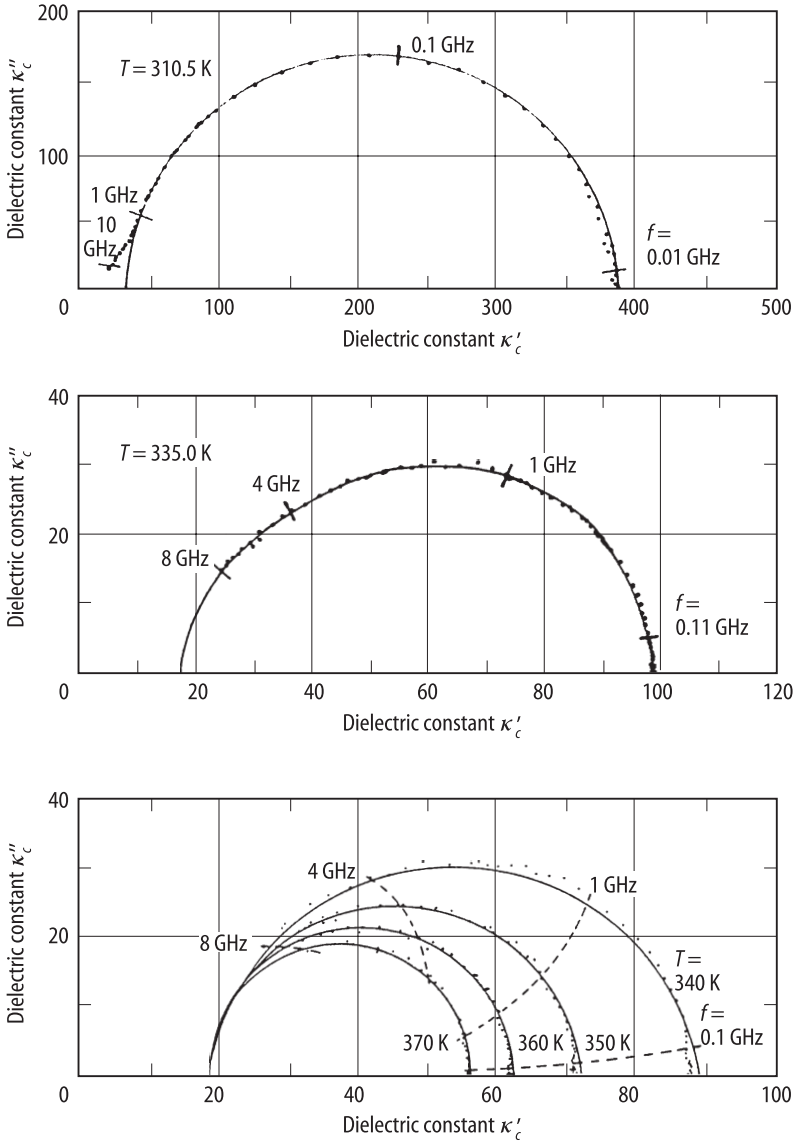

Fig. 57A-2-014. $(CH_3NH_3)_5Bi_2Br_{11}$. Cole-Cole diagram of complex dielectric constant [90Paw]. Parameter: T. $\Theta_{I-I} = 311.5$ K.

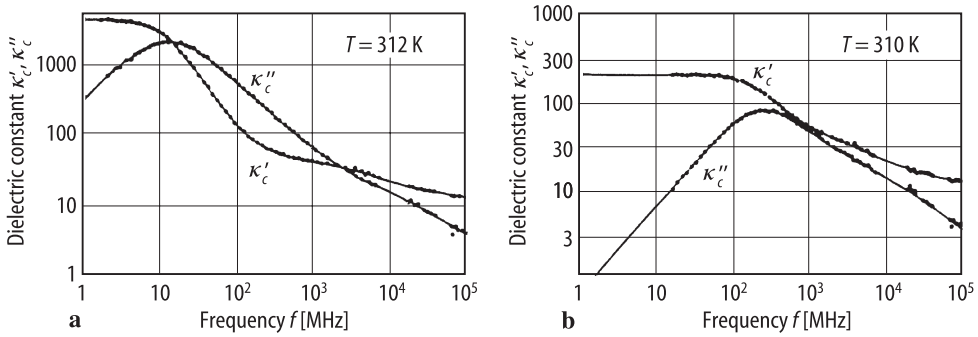

Fig. 57A-2-015. $(CH_3NH_3)_5Bi_2Br_{11}$. κ_c', κ_c'' vs. f at (**a**) $T = 312$ K and (**b**) $T = 310$ K [92Paw1]. $\Theta_{I-I} = 311.5$ K.

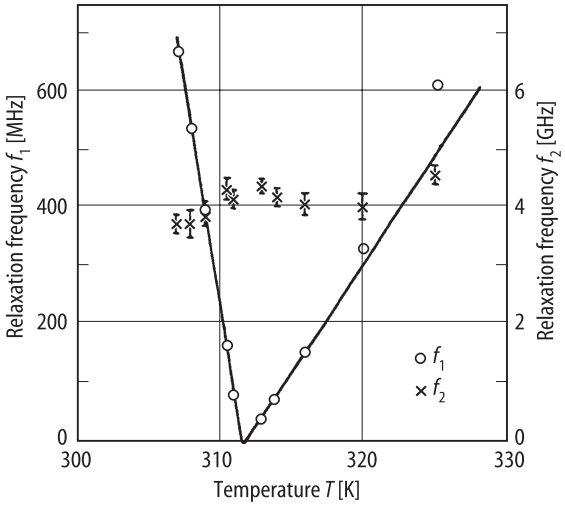

Fig. 57A-2-016. $(CH_3NH_3)_5Bi_2Br_{11}$. f_1, f_2 vs. T [92Paw1]. f_1, f_2: relaxation frequencies of two relaxators.

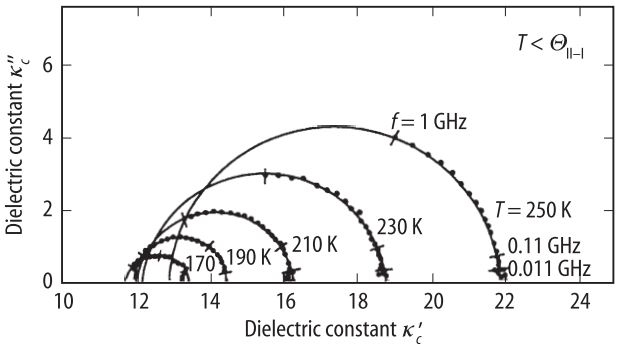

Fig. 57A-2-017. $(CH_3NH_3)_5Bi_2Br_{11}$. Cole-Cole diagram of complex dielectric constant in phase II [92Paw1]. Parameter: T. $\Theta_{II-I} = 311.5$ K.

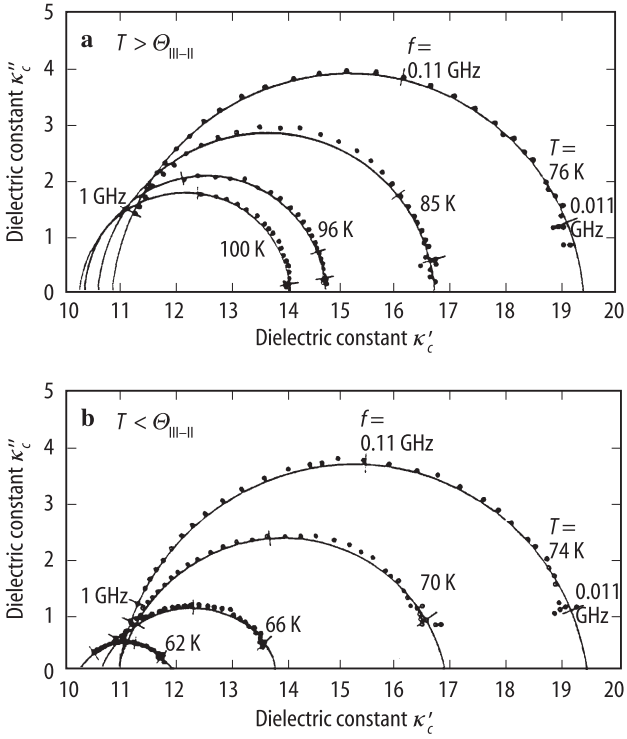

Fig. 57A-2-018. $(CH_3NH_3)_5Bi_2Br_{11}$. Cole-Cole diagram of complex dielectric constant [92Paw1]. Parameter: T. (**a**) $T > \Theta_{III-II}$, (**b**) $T < \Theta_{III-II}$.

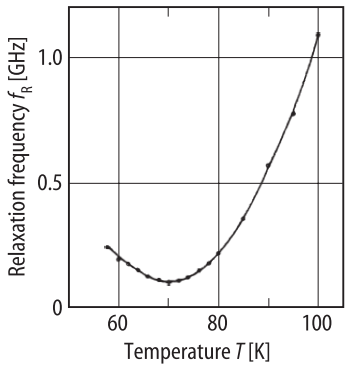

Fig. 57A-2-019. $(CH_3NH_3)_5Bi_2Br_{11}$. f_R vs. T [92Paw1]. f_R: relaxation frequency.

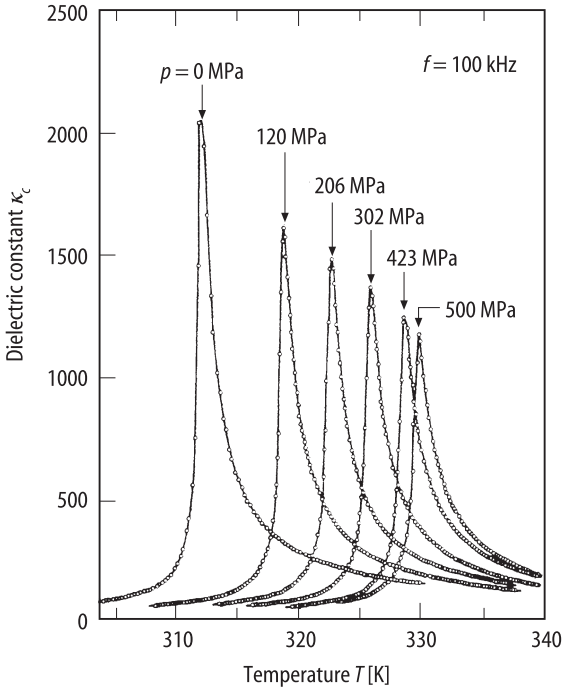

Fig. 57A-2-020. $(CH_3NH_3)_5Bi_2Br_{11}$. κ_c vs. T [95Ges]. Parameter: p. $f = 100$ kHz.

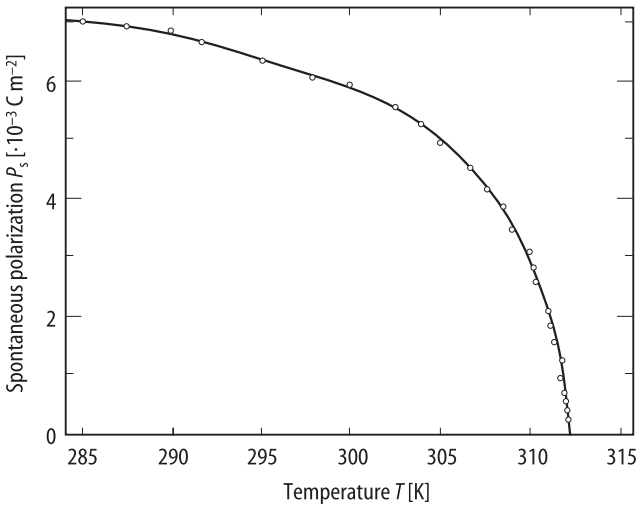

Fig. 57A-2-021. $(CH_3NH_3)_5Bi_2Br_{11}$. P_s vs. T [89Jak1].

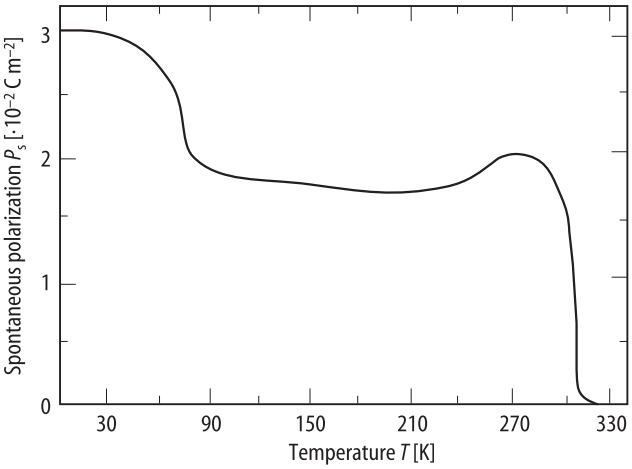

Fig. 57A-2-022. $(CH_3NH_3)_5Bi_2Br_{11}$. P_s vs. T [89Mro].

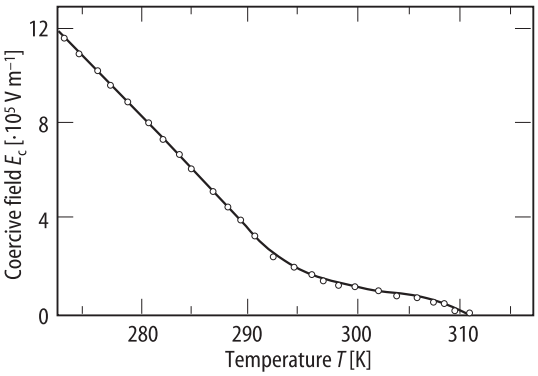

Fig. 57A-2-023. $(CH_3NH_3)_5Bi_2Br_{11}$. E_c vs. T [89Mro].

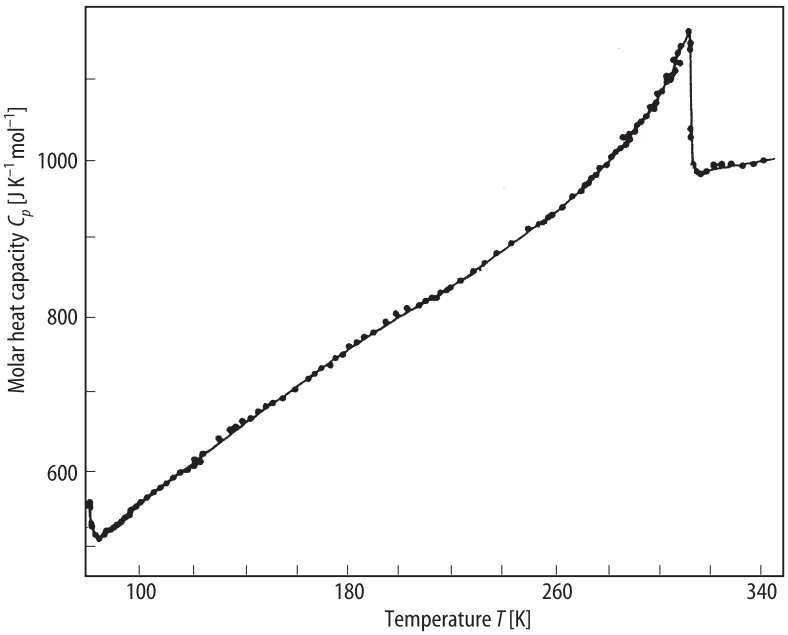

Fig. 57A-2-024. $(CH_3NH_3)_5Bi_2Br_{11}$. C_p vs. T [92Str].

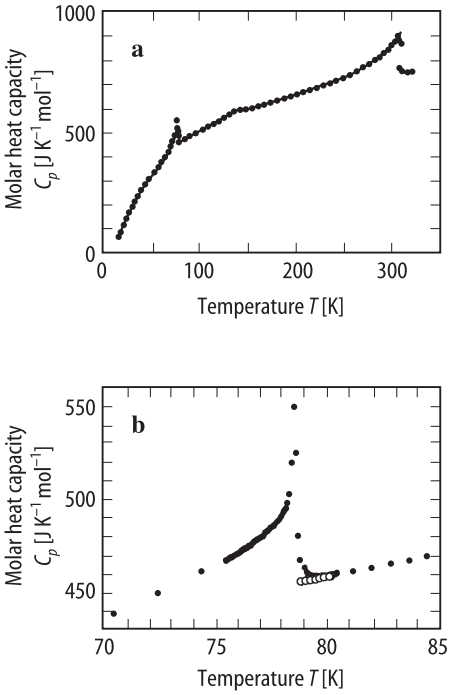

Fig. 57A-2-025. $(CH_3NH_3)_5Bi_2Br_{11}$. C_p vs. T [95Toj]. The data shown by open circles in (**b**) are obtained on heating run after the specimen was cooled just above $\Theta_{III–II}$.

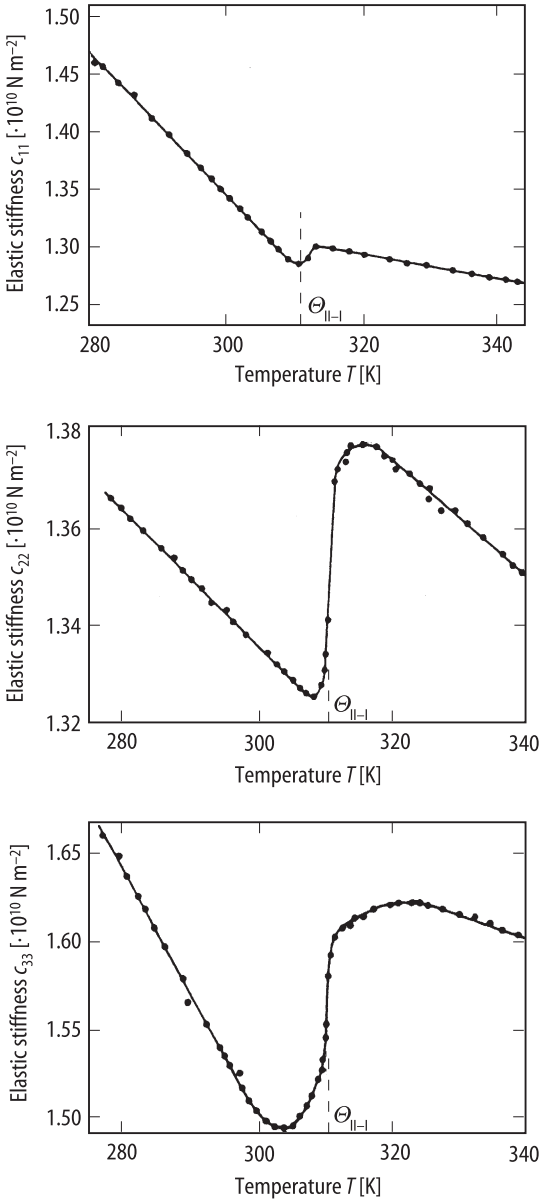

Fig. 57A-2-026. $(CH_3NH_3)_5Bi_2Br_{11}$. c_{11}, c_{22}, c_{33} vs. T [92Jak]. c_{11}, c_{22}, c_{33}: elastic stiffness. Ultrasonic measurement at f = 1.5 MHz.

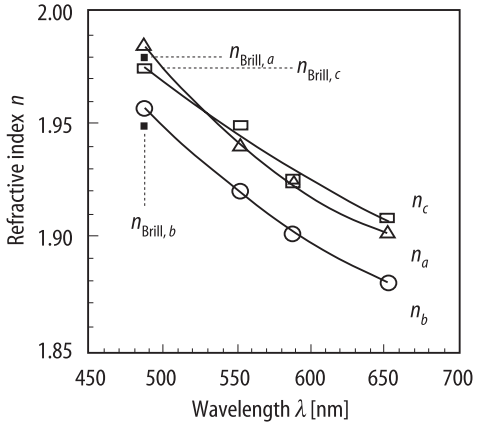

Fig. 57A-2-027. $(CH_3NH_3)_5Bi_2Br_{11}$. n_a, n_b, n_c vs. λ at RT [93Pav]. Optical and Brillouin (denoted as n_{Brill}) measurements.

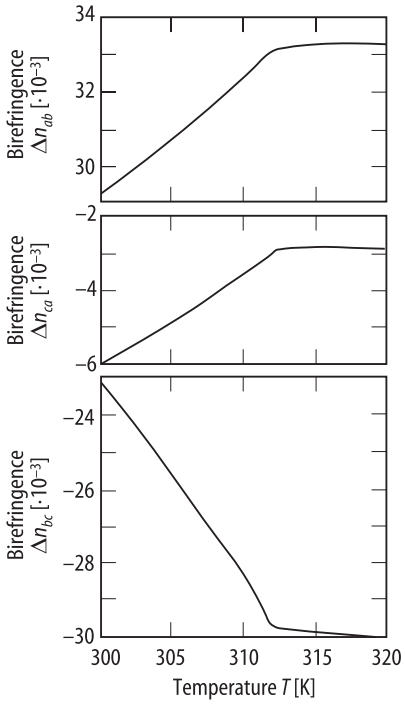

Fig. 57A-2-028. $(CH_3NH_3)_5Bi_2Br_{11}$. Δn_{bc}, Δn_{ca}, Δn_{ab} vs. T [89Kos]. λ = 632 nm. $\Delta n_{bc} = n_b - n_c$, $\Delta n_{ca} = n_c - n_a$, $\Delta n_{ab} = n_a - n_b$. The possibility of interchange of the a and c axes are pointed out in [93Pav] and [95Min].

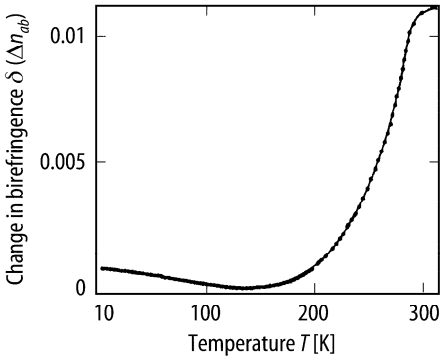

Fig. 57A-2-029. $(CH_3NH_3)_5Bi_2Br_{11}$. $\delta(\Delta n_{ab})$ vs. T [94Prz]. $\delta(\Delta n_{ab})$: change in birefringence in ab plane. $\lambda = 632.8$ nm.

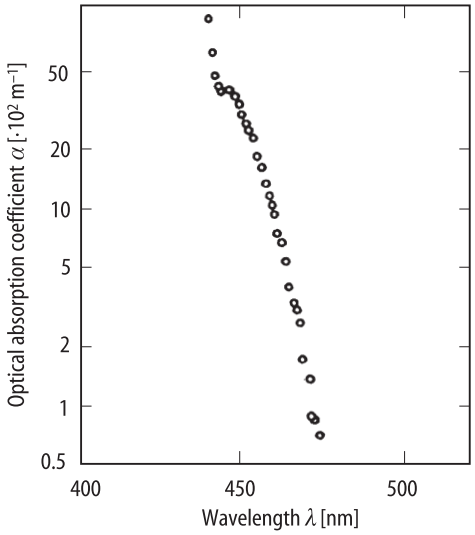

Fig. 57A-2-030. $(CH_3NH_3)_5Bi_2Br_{11}$. α vs. λ at $T = 295$ K [90Min]. α: optical absorption coefficient.

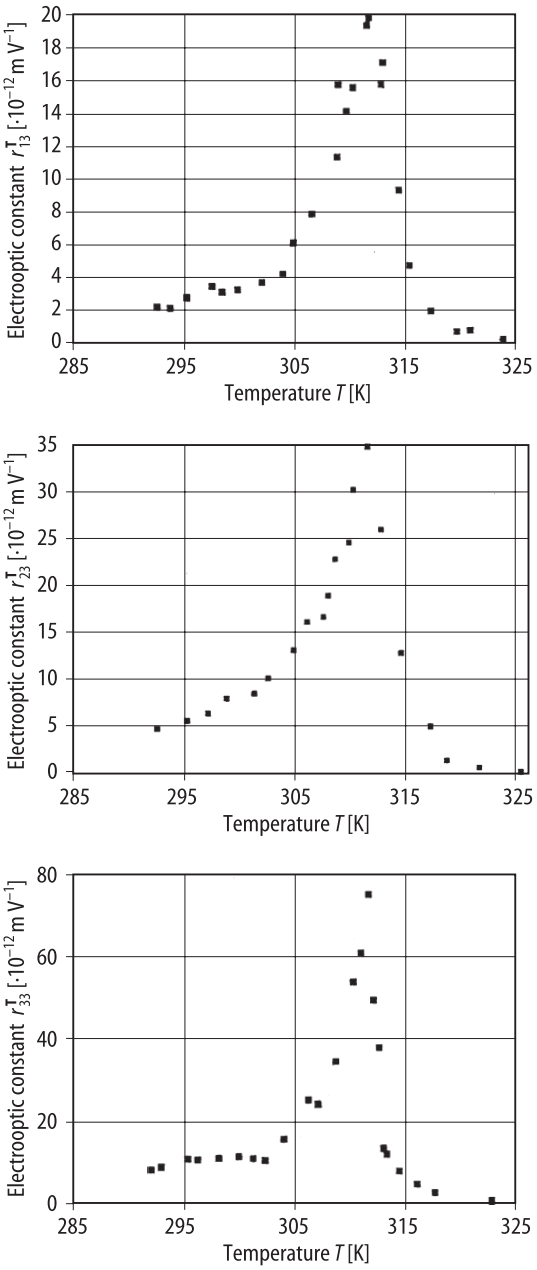

Fig. 57A-2-031. $(CH_3NH_3)_5Bi_2Br_{11}$. $r_{13}^{\mathbf{T}}, r_{23}^{\mathbf{T}}, r_{33}^{\mathbf{T}}$ vs. T [95Min]. $r_{\lambda i}^{\mathbf{T}}$: electrooptic constant for $\boldsymbol{E}$ at stress $\mathbf{T} = 0$. $\lambda = 632.8$ nm. The crystal was driven with rectangular positive voltage pulses with $f = 10$ kHz.

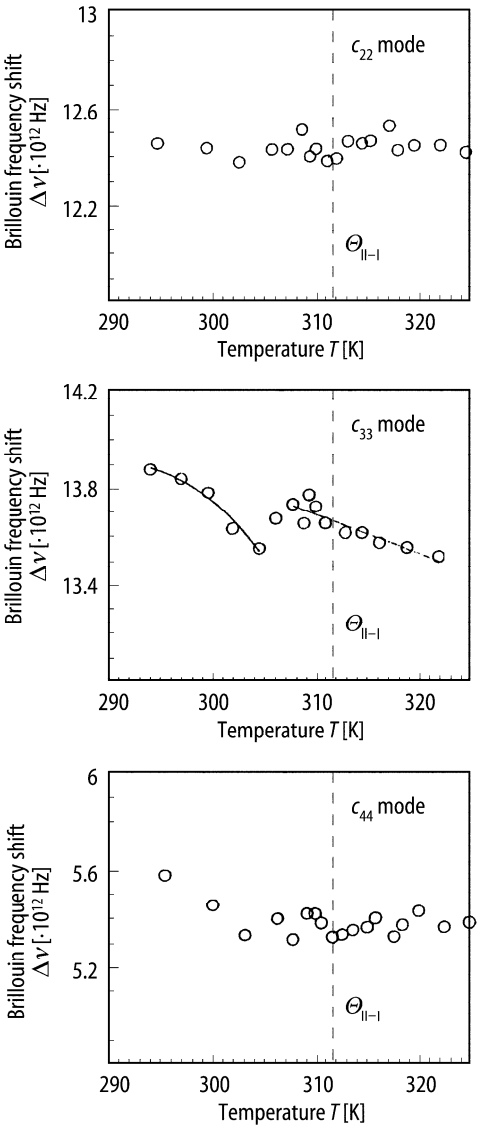

Fig. 57A-2-032. $(CH_3NH_3)_5Bi_2Br_{11}$. $\Delta\nu$ vs. T [93Pav]. $\Delta\nu$: Brillouin frequency shift of the c_{22}, c_{33}, c_{44} acoustic phonon mode. $\lambda = 488$ nm.

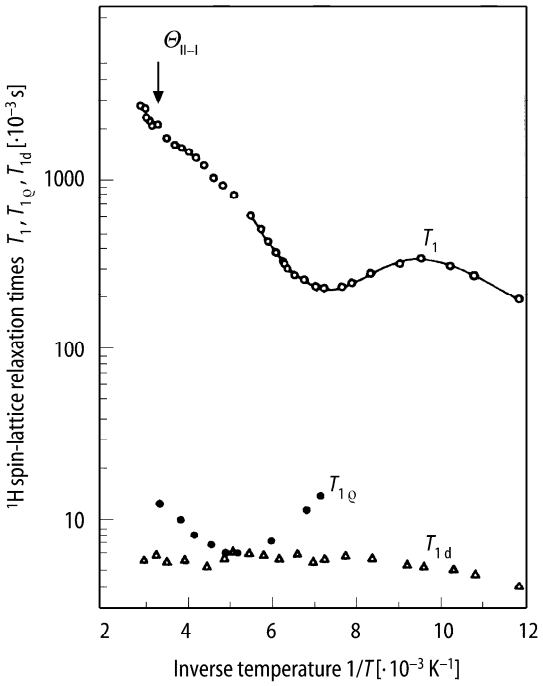

Fig. 57A-2-033. $(CH_3NH_3)_5Bi_2Br_{11}$. T_1, $T_{1\rho}$, T_{1d} vs. $1/T$ [89Pie]. T_1, $T_{1\rho}$, T_{1d}: ^{1}H spin-lattice relaxation time in fixed frame, in rotating frame and in dipolar field, respectively. ν_L = 90 MHz. The spin-locking field B_1 for $T_{1\rho}$ measurement was $10.7 \cdot 10^{-4}$ T.

References

89Jak1 Jakubas, R.: Solid State Commun. **69** (1989) 267.
89Jak2 Jakubas, R., Pykacz, H.: Phys. Status Solidi (a) **115** (1989) K17.
89Jak3 Jakubas, R., Sobczyk, L.: Ferroelectrics **92** (1989) 365.
89Kos Kosturek, B., Jakubas, R.: Phys. Status Solidi (a) **114** (1989) K111.
89Mro Mróz, J., Jakubas, R.: Solid State Commun. **72** (1989) 813.
89Pie Piekara-Sady, L., Jakubas, R., Piślewski, N.: Solid State Commun. **72** (1989) 585.
89Pol Połomska, M., Szcześniak, L., Jakubas, R., Meyer, K.-P., Blumtritt, H.: Ferroelectrics Lett. **10** (1989) 107.
90Bha Bhattacharjee, R., Varma, V., Fernandes, J.R., Rao, C.N.R.: Ferroelectrics Lett. **12** (1990) 79.
90Cac Cach, R., Jakubas, R.: Ferroelectrics **110** (1990) 271.
90Iwa Iwata, M., Ishibashi, Y.: J. Phys. Soc. Jpn. **59** (1990) 4239.
90Jak Jakubas, R., Lefebvre, J.: Ferroelectrics **108** (1990) 115.
90Mat Matuszewski, J., Jakubas, R., Sobczyk, L., Głowiak, T.: Acta Crystallogr. Sect. C **46** (1990) 1385.
90Min Miniewicz, A., Jakubas, R.: J. Mol. Electron. **6** (1990) 113.
90Mro Mróz, J., Poprawski, R., Kolarz, A., Jakubas, R.: Solid State Commun. **76** (1990) 821.
90Paw Pawlaczyk, C., Motsch, H., Jakubas, R., Unruh, H.-G.: Ferroelectrics **108** (1990) 127.
90Pol Połomska, M., Jakubas, R.: Ferroelectrics **106** (1990) 57.
91Min Miniewicz, A., Jakubas, R.: Ferroelectrics **115** (1991) 119.
91Pol Połomska, M., Jakubas, R.: Izv. Akad. Nauk SSSR, Ser. Fiz. **55** (1991) 545; Bull. Acad. Sci. USSR, Phys. Ser. (English Transl.) **55** (1991) 126.
91Sze Szezesniak, L., Meyer, K.-P., Jakubas, R.: Izv. Akad. Nauk SSSR, Ser. Fiz. **55** (1991) 543; Bull. Acad. Sci. USSR, Phys. Ser. (English Transl.) **55** (1991) 123.
92Jak Jakubas, R., Lefebvre, J., Fontaine, H., François, P.: Solid State Commun. **81** (1992) 515.
92Orz Orzechowski, K., Bator, G., Jakubas, R.: Chem. Phys. Lett. **199** (1992) 325.
92Paw1 Pawlaczyk, C., Planta, K., Bruch, C., Stephen, J., Unruh, H.-G.: J. Phys. Condens. Matter **4** (1992) 2687.
92Paw2 Pawlowski, A., Jakubas, R., Ramos, S., Del Cerro, J.: Ferroelectrics **125** (1992) 29.
92Pyk Pykacz, H., Mróz, J., Jakubas, R.: Acta Phys. Pol. A **81** (1992) 667.
92Str Strukov, B.A., Taraskin, S.A., Mróz, J., Poprawski, R.: Fiz. Tverd. Tela **34** (1992) 1860; Sov. Phys. Solid State (English Transl.) **34** (1992) 992.
93Mar Marqueton, Y., Miniewicz, A., Jakubas, R.: Ferroelectrics **145** (1993) 109.
93Pav Pavel, M., Fousková, A., Jakubas, R., Miniewicz, A.: Ferroelectrics **146** (1993) 37.
94Jak Jakubas, R., François, P., Lefebvre, J.: Acta Phys. Pol. A **85** (1994) 579.
94Mat Matyjasek, K., Jakubas, R.: Acta Phys. Pol. A **85** (1994) 835.
94Prz Przeslawski, J., Kosturek, B., Jakubas, R., Lingard, R., Arzt, S., Fitzmaurice, A.: Ferroelectrics **152** (1994) 367.
95Ges Gesi, K., Iwata, M., Ishibashi, Y.: J. Phys. Soc. Jpn. **64** (1995) 2650.
95Mat Matyjasek, K., Jakubas, R.: Ferroelectrics **172** (1995) 201.
95Min Miniewicz, A., Żuk, W., Jakubas, R.: Ferroelectrics **165** (1995) 241.
95Mro Mróz, J., Pykacz, H., Jakubas, R.: Acta Phys. Pol. A **88** (1995) 369.
95Toj Tojo, T., Atake, T., Iwata, M., Ishibashi, Y.: Abstracts of the Meeting of the Phys. Soc. Jpn., 50th Annual Meeting, Yokohama, March, 1995, Pt. 2, 76.
95Tom Tomaszewski, P.E.: Phys. Status Solidi (a) **152** (1995) K7.
96Ges Gesi, K., Iwata, M., Ishibashi, Y.: J. Phys. Soc. Jpn. **65** (1996) 14.